Pharmacological Brake-Release of mRNA Translation Enhances Cognitive Memory

Carmela Sidrauski[1], Diego Acosta-Alvear[1], Arkady Khoutorsky[2], Punitha Vedantham[3], Brian R. Hearn[3], Han Li[4], Karine Gamache[5], Ciara Gallagher[1], Kenny K-H. Ang[3], Chris Wilson[3], Voytek Okreglak[1], Avi Ashkenazi[4], Byron Hann[6], Karim Nader[5], Michelle R. Arkin[3], Adam R. Renslo[3], Nahum Sonenberg[2] and Peter Walter[1]

[1]Department of Biochemistry and Biophysics, Howard Hughes Medical Institute, University of California, San Francisco, United States; [2]Department of Biochemistry and McGill Cancer Center, Montreal, Quebec, Canada; [3]Small Molecule Discovery Center and Department of Pharmaceutical Chemistry, University of California, San Francisco, United States; [4]Department of Molecular Oncology, Genentech Inc., South San Francisco, California, United States; [5]Department of Psychology, McGill University, Montreal, Quebec, Canada; [6]Helen Diller Family Comprehensive Cancer Center, University of California, San Francisco, United States

Abstract

Phosphorylation of the α-subunit of initiation factor 2 (eIF2α) controls protein synthesis by a conserved mechanism. In metazoa, distinct stress conditions activate different eIF2α kinases (PERK, PKR, GCN2, and HRI) that converge on phosphorylating a unique serine in eIF2α. This collection of signaling pathways is termed the "integrated stress response" (ISR). eIF2α phosphorylation diminishes protein synthesis, while allowing preferential translation of some mRNAs. Starting with a cell-based screen for inhibitors of PERK signaling, we identified a small molecule, named ISRIB, that potently (IC_{50}=5 nM) reverses the effects of eIF2α phosphorylation. ISRIB reduces the viability of cells subjected to PERK-activation by chronic endoplasmic reticulum stress. eIF2α phosphorylation is implicated in memory consolidation. Remarkably, ISRIB-treated mice display significant enhancement in spatial and fear-associated learning. Thus, memory consolidation is inherently limited by the ISR, and ISRIB releases this brake. As such, ISRIB promises to contribute to our understanding and treatment of cognitive disorders.

Introduction

In metazoa, diverse stress signals converge at a single phosphorylation event at serine 51 of a common effector, the translation initiation factor eIF2α. This step is carried out by four eIF2α kinases in mammalian cells: PERK, which responds to an accumulation of unfolded proteins in the endoplasmic reticulum (ER), GCN2 to amino acid starvation and UV light, PKR to viral infection, and HRI to heme deficiency. This collection of signaling pathways has been termed the "integrated stress response" (ISR), as they converge on the same molecular event. eIF2α phosphorylation results in an attenuation of translation with consequences that allow cells to cope with the varied stresses (1).

eIF2 (which is comprised of three subunits, α, β and γ) binds GTP and the initiator Met-tRNA to form the ternary complex (eIF2-GTP-Met-$tRNA_i$), which, in turn, associates with the 40S ribosomal subunit forming the 43S pre-initiation complex (PIC) that scans the 5'UTR of mRNAs to select the initiating AUG codon. Upon phosphorylation of its α-subunit, eIF2 becomes a competitive inhibitor of its GTP-

exchange factor (GEF), eIF2B (2). The tight and non-productive binding of phosphorylated eIF2 to eIF2B prevents loading of the eIF2 complex with GTP thus blocking ternary complex formation and reducing translation initiation (3). Because eIF2B is less abundant than eIF2, phosphorylation of only a small fraction of the total eIF2 has a dramatic impact on eIF2B activity in cells.

Paradoxically, under conditions of reduced protein synthesis, a small group of mRNAs that contain upstream open reading frames (uORFs) in their 5'UTR are translationally up-regulated (4,5). These include mammalian ATF4 (a cAMP element binding (CREB) transcription factor) and CHOP (a pro-apoptotic transcription factor) (6-8). ATF4 regulates the expression of many genes involved in metabolism and nutrient uptake and additional transcription factors, such as CHOP, which is under both translational and transcriptional control (9). Phosphorylation of eIF2α thus leads to preferential translation of key regulatory molecules and directs diverse changes in the transcriptome of cells upon cellular stress.

One of the eIF2α kinases, PERK, lies at the intersection of the ISR and the unfolded protein response (UPR) that maintains homeostasis of protein folding in the ER (10). The UPR is activated by unfolded or misfolded proteins that accumulate in the ER lumen because of an imbalance between protein folding load and protein folding capacity, a condition known as "ER stress". In mammals, the UPR is comprised of three signaling branches mediated by ER-localized transmembrane sensors, PERK, IRE1, and ATF6. These sensor proteins detect the accumulation of unfolded protein in the ER and transmit the information across the ER membrane, initiating unique signaling pathways that converge in the activation of an extensive transcriptional response, which ultimately results in ER expansion (11). The lumenal stress-sensing domains of PERK and IRE1 are homologous and likely activated in analogous ways by direct binding to unfolded peptides (12). This binding event leads to oligomerization and *trans*-autophosphorylation of their cytosolic kinase domains, and, for PERK, phosphorylation of its only known substrate, eIF2α. In this way, PERK activation results in a quick reduction in the load of newly synthesized proteins that are translocated into the ER-lumen (13).

Upon ER stress, both the transcription factor XBP1s, produced as the consequence of a non-conventional mRNA splicing reaction initiated by IRE1, and the transcription factor ATF6, produced by proteolysis and release from the ER membrane, collaborate with ATF4 to induce the vast UPR transcriptional response. Transcriptional targets of the UPR include the ER protein folding machinery, the ER-associated degradation machinery, and many other components functioning in the secretory pathway (14). Although the UPR initially mitigates ER stress and as such confers cytoprotection, persistent and severe ER stress leads to activation of apoptosis that eliminates damaged cells (15,16).

By interrogating a large chemical library for small molecules that block PERK signaling, we identified ISRIB as a potent ISR inhibitor, functioning downstream of all eIF2α kinases. ISRIB proves a powerful tool to explore the consequences of acute inhibition of the ISR in cells and animals.

Results

Design of cell-based screen for inhibitors of PERK signaling

To identify inhibitors of PERK signaling, we engineered a reporter that allows monitoring of PERK activation in living cells. To this end, we constructed a retroviral vector containing the open-reading frame of firefly luciferase fused to the 5'UTR of ATF4 mRNA (Fig. 1a), which contains two short open-reading frames (uORFs) that control ATF4 translation in a stress-dependent manner. After infection, we established a HEK293T cell line harboring the stably integrated reporter. We used thapsigargin, a potent ER stressor that inhibits the ER calcium pump, to activate PERK and induce eIF2α phosphorylation. Thapsigargin treatment resulted in a 4.9-fold induction in luciferase activity in a 384 well format with a Z factor of 0.5 (Fig. 1b). This format was used to screen 106,281 compounds covering a wide chemical space. We identified 460 hits (0.43%) (Fig. 1c), which were further validated in an 8-point dose-response assay using the same reporter. We further triaged the compounds by discarding inhibitors that also affected the IRE1 branch of the UPR using a luciferase-based XBP1 splicing reporter. Less than half (187 hits) of our initial hits proved unique to the PERK branch. We next used an orthogonal secondary screen that employed a different reporter (bi-cistronic ATF4-dGFP-IRES-mCherry) stably integrated into a different cell line (U2OS cells). The read-out of this latter screen was microscopy-based, which allowed us to simultaneously assess acute toxicity by cell counting, further reducing the number of viable hits to 77 (data not shown). As a tertiary screen, we tested compounds for their ability to inhibit ER stress-elicited induction of endogenous ATF4 by Western blot analysis. Twenty-eight compounds passed this test and were analyzed further.

A symmetric bisglycolamide, ISRIB, is a potent inhibitor of PERK signaling

One of the 28 compounds was of particular interest because of its high potency in cells (library compound IC_{50} = 40 nM). This compound (henceforth referred to as "ISRIB" for Integrated Stress Response inhibitor) is a symmetric bis-glycolamide, containing a central bi-substituted cyclohexane, and can exist as two diastereomers, *cis* and *trans* (Fig. 2a). We synthesized both isomers and tested their ability to inhibit the ATF4-luciferase reporter (Fig. 2b). *Trans*-ISRIB proved 100-fold more potent (IC_{50} = 5 nM) than *cis*-ISRIB (IC_{50} = 600 nM), indicating that the compound's interaction with its cellular target is stereospecific. Given the two-order-of-magnitude difference in activity in this assay, the measured activity of *cis*-ISRIB may be an over-estimate, as we cannot exclude a small contamination with *trans*-ISRIB, which is far more potent. The lower IC_{50} of *trans*-ISRIB relative to the compound in the small molecule library indicates that the library likely contains a mixture of the two stereoisomers. All further experiments in this study were carried out with the synthesized *trans*-isomer of ISRIB.

ISRIB is PERK-branch specific but does not impair PERK phosphorylation

We next determined at which step ISRIB blocks ATF4 production. To this end, we first probed the phosphorylation status of PERK by Western blotting. PERK phosphorylation is indicative of its activation by autophosphorylation and can be

recognized by reduced mobility on SDS-polyacrylamide gels. Notably, ISRIB did not inhibit the mobility shift of PERK observed in ER-stressed cells (Fig. 2c). Rather, we observed an exaggerated mobility shift, indicative of increased phosphorylation of PERK upon ER stress, induced by either thapsigargin or tunicamycin (an inhibitor of *N*-linked glycosylation). In each case, in the absence of ISRIB, ATF4 and XBP1s were produced upon ER stress induction. In agreement with the behavior of the reporters described above, ISRIB blocked production of endogenous ATF4, whereas XBP1 mRNA splicing (Fig. 2d) and XBP1s production persisted (Fig. 2c and Fig. 3 supplement 1). As shown below (cf. Fig. 5d), ISRIB also did not affect activation of the ATF6-branch of the UPR. We conclude that ISRIB specifically blocks signaling of the PERK-branch of the UPR.

ISRIB-treated cells are resistant to eIF2α phosphorylation

Given that PERK phosphorylation was not diminished in ISRIB-treated, ER-stressed cells, we next directly assessed eIF2α phosphorylation. We measured the levels of phosphorylated eIF2α using an antiphospho-eIF2α antibody-based assay to quantify phosphorylation at serine 51 (see Methods). Upon induction of ER stress by tunicamycin or thapsigargin, phosphorylation of eIF2α increased over time, reaching a 4- and 7-fold increase after 120 minutes respectively (Fig. 3a). Unexpectedly, ISRIB did not block eIF2α phosphorylation under either of these ER stress-inducing conditions. On the contrary, 120 min after tunicamycin addition, ISRIB further increased the level of eIF2α phosphorylation, approaching that obtained with thapsigargin. ISRIB alone had no effect on eIF2α phosphorylation. These results indicate that ISRIB blocks effects downstream of PERK and eIF2α phosphorylation.

One way of explaining why ISRIB blocks ATF4 production yet leaves eIF2α phosphorylation intact is by rendering cells insensitive to the effects of this phosphorylation event. In agreement with this notion, ISRIB sustained global translation (as monitored by ^{35}S-methionine incorporation into newly synthesized polypeptides) even in the presence of ER stress (Fig. 3b). After thapsigargin treatment, cells experienced a 40% drop in translation, which was abolished by ISRIB. As predicted by this result, extracts prepared from mouse embryonic fibroblasts (MEFs) experiencing ER stress showed a pronounced increase in the 80S monosomes at the expense of polyribosomes (Fig. 3c), which was reversed (at least partially) by addition of ISRIB. We chose MEFs for this analysis because they show stronger translational inhibition in response to ER stress than HEK293T cells. ISRIB was the only molecule in our collection of 28 hits that reversed translational attenuation upon ER-stress.

Under normal growth conditions, an abundance of 43S pre-initiation complexes (PICs) leads to mRNAs loaded with a small ribosomal subunit in addition to fully assembled ribosomes. The presence of PICs on an mRNA can be detected as “halfmer” peaks on polysome gradients. In the gradients shown in Fig. 3c, addition of a PIC to disomes and trisomes was well resolved (enlarged in Fig. 3 supplement 4). Upon eIF2α phosphorylation in ER-stressed cells, the reduction in PIC resulted in disappearance of the halfmer population. As expected, the disappearance of the halfmer peak upon ER-stress was dependent on eIF2α phosphorylation as no reduction was observed in MEFs

that solely express non-phosphorylatable eIF2α(S51A) (Fig. 3 supplement 5). Importantly, ISRIB partially restored the halfmer population in ER-stressed cells, providing support to the notion that it helps maintain high PIC levels even when eIF2α is phosphorylated (Fig. 3 supplement 4). These data indicate that ISRIB exerts its function by maintaining elevated ternary complex levels.

To further ascertain that cells treated with ISRIB are resistant to the effects of eIF2α phosphorylation, we transduced an inducible phospho-mimetic allele of eIF2α in which serine 51 was changed to an aspartic acid (S51D) into HEK293T cells. Expression of this allele upon doxycycline addition induced translational attenuation (Fig. 3d) as seen by an increase in the 80S peak and a decrease in the polysome population. ISRIB rescued translation returning it to the levels observed in non-induced cells. In conclusion, ISRIB restores translation in cells containing either phospho-eIF2α or eIF2α(S51D), thereby excluding any pleiotropic effects that might have been caused by the reagents used to activate ER stress.

To rule out that ISRIB exerts non-specific effects on translation independent of eIF2α phosphorylation, we tested whether ISRIB reverses a translational block in CAP-mediated initiation. To this end we used Torin-1, an inhibitor of mTOR that blocks phosphorylation of 4E-BP1 and S6K1, and leads to translational attenuation (17). Addition of Torin-1 to MEFs led to an increase in the 80S peak and reduction in the polysome population to a similar extent as shown above in cells treated with ER stressors or expressing eIF2α(S51D) (Fig. 3e, compare with 3c and 3d). In contrast to these treatments, addition of ISRIB did not reverse the effect of Torin-1 on translation. Therefore, the ability of ISRIB to block translational attenuation is specific to eIF2α phosphorylation.

If ISRIB makes cells insensitive to eIF2α phosphorylation, it should not matter which kinase phosphorylates eIF2α. To test this prediction, we subjected cells to amino acid starvation, which activates the eIF2α kinase GCN2 and leads to ATF4 production. In addition, we used a recently identified small molecule activator to induce eIF2α phosphorylation by activating HRI, another eIF2α kinase (18). As expected, ISRIB blocked ATF4 induction after activation of either GCN2 or HRI (Fig. 3f). Under both conditions, PERK was not activated as shown by a lack of mobility shift. These data suggest that ISRIB is a *bona fide* ISR inhibitor that blocks signaling downstream of all eIF2α kinases.

Both CHOP and GADD34 are transcriptional targets of ATF4. Thus, blocking ATF4 accumulation with ISRIB should result in a reduction in the transcriptional induction of the mRNAs encoding these targets. As shown in Figure 4a, GADD34 and CHOP mRNAs accumulated in ER-stressed U2OS cells, and ISRIB significantly reduced their induction. In agreement, we observed no CHOP accumulation after induction of ER stress in ISRIB-treated cells (Fig. 4b). Thus ISRIB impairs the transcriptional network governed by ATF4 during the ISR.

ISRIB impairs adaptation to ER stress

As previously shown, cells homozygous for non-phosphorylatable eIF2α, eIF2α(S51A), are unable to cope with ER stress properly, leading to reduced viability (19). This indicates that events downstream of eIF2α phosphorylation are required to resolve the stress. As shown in Figure 5a, ISRIB treatment of wild-type cells had similar consequences. Importantly, addition of ISRIB alone did not affect cell viability, as judged by the number of colonies that form after acute treatment. By contrast, ISRIB addition caused a strong synergistic effect on ER-stressed cells, reducing colony number and size significantly more than ER-stress alone. This reduction in cell survival resulted from activation of apoptosis as the activity of the executioner caspases 3 and/or 7 was significantly induced under these conditions (Fig. 5b) (20).

The notion that ER stress remains unmitigated in ISRIB-treated cells is supported by sustained activation of all three UPR sensors. First, as shown in Figure 2c, PERK was hyper-phosphorylated. Second, cells expressing an IRE1-GFP fusion protein showed prolonged foci formation (Fig. 5c), indicative of IRE1 oligomerization. Third, we observed prolonged ER stress-induced proteolytic processing of ATF6 (Fig. 5d). Importantly, in the absence of ER stress ISRIB treatment alone did not induce any of these sensors (Fig. 3 supplement 1, Fig. 5c and data not shown).

ISRIB increases long-term memory in rodents

eIF2α(+/S51A) heterozygote mice display enhanced memory, while induction of the eIF2α kinase PKR in brain pyramidal cells impairs memory (21,22). Based on these observations, we wondered whether treatment of mice with ISRIB would affect memory. ISRIB showed favorable properties in pharmacokinetic profiling experiments indicating sufficient bioavailability for *in vivo* studies. ISRIB displayed a half-life in plasma of 8h (Fig. 6a) and readily crossed the blood-brain barrier, quickly equilibrating with the central nervous system (Fig. 6b). After a single intraperitoneal injection, we detected ISRIB in the brain of mice at concentrations several fold higher than its IC_{50} (24 h after injection, the ISRIB concentration in the brain was approximately 60 nM). To explore ISRIB's effects on memory, we injected mice intraperitoneally with ISRIB and tested hippocampus-dependent spatial learning. To this end, we trained mice in a Morris water maze, in which animals learn to associate visual cues with the location of a submerged hidden platform. Because we were looking for memory enhancement, we used a weak training protocol. As shown in Figure 6c, ISRIB-treated mice reached the hidden platform significantly faster (escape latency after 5 days of training = 16.4 +/- 4.8 s) compared to vehicle treated controls (68.1 +/- 20 s, $p < 0.05$). The difference was already pronounced by days 3 and 4. In agreement with these results, ISRIB-treated mice significantly preferred the target quadrant in a "probe test" conducted at the end of the training sessions, in which the platform was removed from the pool ($p < 0.05$; Fig. 6d) and showed increased crossing of the platform location ($p < 0.05$; Fig. 6e).

We next tested contextual fear conditioning, which represents a different kind of hippocampus-dependent learning in which eIF2α phosphorylation has also been implicated to play a role (22). In these experiments, we paired a particular environmental context (a different cage) with a foot shock. In this case the context acts as the "conditioned stimulus, CS" and is associated with the foot shock, the "unconditioned

stimulus, US". ISRIB-treated mice showed increased freezing upon presentation of the conditioned environment 24 h after training as compared to vehicle treated mice ($p < 0.05$; Fig. 6f). No differences were observed in short-term memory (1 h) between these two treatments. Taken together, we conclude that treatment with ISRIB enhances both hippocampus-dependent spatial learning and hippocampus-dependent contextual fear conditioning.

To test learning associated with a different region of the brain, we explored the effects of ISRIB on auditory fear conditioning, which depends on the amygdala. In this type of learning a tone (CS) is paired with a foot shock (US). In these experiments, we injected ISRIB or vehicle directly into the amygdala of rats via cannulation. ISRIB-treated rats showed a significant increase over vehicle-injected rats in the level of freezing when presented with the tone (CS) at 24 h (long-term memory, $p < 0.05$; Fig. 6g). By contrast, we observed no difference between ISRIB- and vehicle-treated rats at 3 h (short-term memory). As expected, both ISRIB- and vehicle-treated rats showed similar freezing responses prior to training (pre-CS). Taken together, these data suggest that long-term memory is selectively enhanced in ISRIB-treated animals.

Discussion

We identified a novel small molecule, ISRIB, that renders cells resistant to the effects of eIF2α phosphorylation, restoring the cell's translation capacity. ISRIB is the first reported antagonist of the ISR. It acts as a potent and stereospecific inhibitor with an IC_{50} of 5 nM in cultured cells, suggesting a specific and tight interaction with its cellular target. By blocking signaling through the PERK branch of the UPR, ISRIB prevents cells from re-establishing ER homeostasis. Unmitigated ER stress synergizes with ISRIB to induce apoptosis. ISRIB shows good pharmacokinetic properties, readily crosses the blood-brain barrier, and exhibits no overt toxicity in mice, making it suitable for *in vivo* studies. As such, ISRIB emerges as a powerful tool to explore the roles of the UPR and the ISR in disease models and physiological processes. In particular, we utilized ISRIB to show that overriding the consequences of eIF2α phosphorylation enhances memory consolidation in rodents, suggesting an important role of eIF2α phosphorylation in modulating higher-order brain function.

Molecular Action of ISRIB

The structure of ISRIB provides no insights as to its target in cells. To date, we have synthesized and assayed more than 75 analogs, which demonstrate a tractable structure-activity relationship (to be published elsewhere). The analyses have identified sites on the molecule where affinity tags and/or crosslinking moieties can be added, which promise to aid in target identification. Based on previous insights on how cells can become resistant to eIF2α phosphorylation, we consider two likely scenarios by which ISRIB could act:

- First, ISRIB could weaken the effects of the non-productive interaction of phospho-eIF2α with eIF2B, thereby increasing the available eIF2α-GEF activity in the cell, restoring the concentration of ternary complex that can engage in translation initiation. Precedence for this possibility derives from genetic studies in *S. cerevisiae*,

where the molecular mechanism of regulation by eIF2α phosphorylation was first discovered. As in mammalian cells, amino acid starvation in yeast leads to GCN2 activation and eIF2α phosphorylation, resulting in overall translational down-regulation and translational induction of a transcriptional activator, GCN4, mediated by uORFs in the 5'UTR of its mRNA (4). eIF2B is a conserved protein complex comprised of five different subunits, two of which form the catalytic core, and the remaining three have regulatory roles. Mutations in different eIF2B subunits can elicit a phospho-eIF2α resistant phenotype (23-25). These mutations have been proposed to act either by weakening the interaction of phospho-eIF2α with eIF2B, reducing its ability to outcompete non-phosphorylated eIF2 for binding, or by allowing binding of phospho-eIF2α to the mutant eIF2B in a manner that is conducive to nucleotide exchange. ISRIB could be altering the affinity of phospho-eIF2α for eIF2B or overcoming the nonproductive interaction that blocks GTP loading, mimicking the effect of these mutations.

- Second, ISRIB could increase the activity of eIF2B, so that the residual amount not engaged with phospho-eIF2α is sufficient to sustain normal levels of ternary complex. Precedence for this possibility derives from studies in macrophages, where engagement of toll-like receptor (TLR) 4 results in activation of the catalytic activity of eIF2B (26). This activation results from engagement of the TLR-signaling pathway that induces a phosphatase removing a constitutively present inhibitory phosphate from the eIF2B ε-subunit (S539). Pathogens utilize this mechanism to circumvent translational attenuation and CHOP production under prolonged stress-inducing conditions (27). ISRIB did not reduce phosphorylation of S539 in the eIF2B ε-subunit (Fig. 3 supplement 1), indicating that it does not utilize this particular regulatory phosphorylation to increase GEF activity. However, ISRIB may modulate other post-translational modifications that impinge on the activity of eIF2B.

ISRIB can influence cell fate

As a signaling network with interconnected signaling branches, the UPR exhibits both cytoprotective and pro-apoptotic functions. When faced with ER stress, PERK-mediated translational attenuation contributes to adaptation by reducing the load of newly synthesized proteins that are translocated into the ER (13). In addition, induction of the transcription regulator ATF4 upregulates many genes that increase the protein folding capacity in the ER. Both of these activities serve to reestablish homeostasis, balancing the protein folding load and protein folding capacity in the ER lumen. This reasoning is supported by the increased sensitivity to ER stress exhibited by MEFs that lack PERK or ATF4, as well as MEFs that carry a non-phosphorylatable knock-in allele of eIF2α(S51A) (13,19,28). In agreement, we show that ISRIB decreases the viability of cells that are subjected to ER-stress. In these cells, ISRIB sustains IRE1 and ATF6 activation, indicating that ER stress remains unmitigated in the absence of PERK signaling. As some cancer cells sustain an activated UPR to aid in their survival, ISRIB could provide a new therapeutic approach to cancer chemotherapy. In agreement, a PERK-specific inhibitor demonstrates antitumor activity in a human pancreatic tumor xenograft model (29). The deleterious synergistic effect between ER-stress and ISRIB may be generally advantageous to kill cancer cells, especially those derived from

secretory lineages that have increased secretory load and increased basal levels of ER stress (including myelomas, and pancreatic and breast cancers).

Importantly, by acting downstream of eIF2α phosphorylation, ISRIB blocks multiple stress effectors (i.e., all eIF2α kinases). During tumor growth, hypoxic conditions and a lack of nutrients can activate both PERK and GCN2, and PERK $^{-/-}$ or GCN2 $^{-/-}$ MEFs give rise to significantly smaller tumors in mouse xenograft models than their wild-type counterparts (30,31). Hence both kinases have pro-survival roles in tumor development. By blocking signaling by both kinases, ISRIB displays unique properties that may be beneficial in reducing cellular fitness of tumor cells.

ISRIB and brain function

The importance of eIF2 / eIF2B function in the human brain is underscored by familial diseases caused by mutations in these factors. One example is Childhood Ataxia with CNS Hypomyelination (CACH), also known as Vanishing White Matter disease (VWM), which has been mapped to mutations in different subunits of eIF2B (32). A second example links a familial intellectual disability syndrome to a mutation in the γ-subunit of eIF2 complex (33).

Several lines of genetic evidence in mice suggest that phosphorylation-dependent regulation of eIF2α phosphorylation is a critical hub for the control of synaptic plasticity (as assessed by late long-term potentiation (L-LTP) in brain slices) and memory consolidation (as assessed in behavioral tasks in animals). In particular, the threshold for induction of L-LTP is reduced and memory consolidation is enhanced in mice lacking GCN2 or PKR and in mice heterozygous for non-phosphorylatable eIF2α(S51A), which have reduced levels of eIF2α phosphorylation (22,34,35). As we show here, ISRIB pharmacologically phenocopies these genetic manipulations in behavioral tasks by rendering cells insensitive to eIF2α phosphorylation. In agreement, treatment of mice with a PKR inhibitor was reported to enhance memory consolidation, and, conversely, treatment with salubrinal, an inhibitor that prolongs eIF2α phosphorylation, to block L-LTP and memory consolidation (22,35).

eIF2α phosphorylation results in a dual effect on gene expression: a global translational diminution and translational upregulation of select mRNA, including ATF4 mRNA. Both may be important to explain the observed effects on L-LTP and memory. It has long been appreciated that new protein synthesis is required for memory consolidation and that ATF4 represses CREB-mediated transcription of "memory genes"(36,37). Indeed, this latter function of ATF4 in memory consolidation is evolutionarily conserved from Aplysia to rodents (38-40). Because a small physiological increase in the level of eIF2α phosphorylation that does not significantly alter overall translation is sufficient to induce ATF4, production of this transcription factor can be finely tuned in neuronal cells by perhaps selective activation of different eIF2α kinases. The observed effects of ISRIB may therefore result from overcoming effects caused by a relatively small level of regulatory phosphorylation that is distinct from the high level resulting from ER stress-inducing agents. In light of this reasoning, a therapeutic window

may exist in which ISRIB's effects as memory enhancer can be exploited without encountering long-term toxic consequences.

ISRIB increases memory consolidation, allowing pharmacological enhancement of the brain's ability to learn. Evolution therefore did not arrive at a maximally optimized process, imposing a brake (via eIF2α phosphorylation) on memory consolidation. This mechanism may underscore the importance of filtering memories before committing them to long-term storage. Indeed, eIF2α phosphorylation also plays a role in dynamic restructuring of memory, as indicated by studies showing that ablation of PERK in the brain impairs behavioral flexibility (41). Our findings raise the possibility that ISRIB or compounds with related activities could serve as invaluable tools in deciphering these higher order brain functions and perhaps be beneficial as a therapeutic agent effecting memory improvement in diseases associated with memory impairment.

Acknowledgments

We thank Yong Huang and Blake Aftab for mass spectrometry and pharmacokinetic analysis and the members of the Walter lab for critical reading of the manuscript. We thank Paige Nittler for her help coordinating this collaboration, and Marc Shuman for his invaluable advice and guidance. This work was funded through an HHMI Collaborative Innovation Award. We thank the HHMI leadership for establishing this visionary funding mechanism, without which this work would not have been possible. DAA was supported by the Irvington Institute Postdoctoral Fellowship of the Cancer Research Institute. AK and NS were supported by the Canadian Institutes of Health Research (N.S., MOP-114994). KKHA was funded by the QB3-Malaysia Program. PW is an Investigator of the Howard Hughes Medical Institute.

Author contributions

CS, Conception and design, acquisition of data, analysis and interpretation of the data, writing the manuscript; DA, Conception, design and construction of reporters and S51D-eIF2α inducible cell lines, analysis of data; AK and NS, Memory studies conception and design, acquisition and analysis of data; KG and KN, Fear conditioning experiments in rats; PV, BRH and ARR, Chemistry design and analysis of data; CG, Construction and characterization of tagged ATF6 cell line, data acquisition; KKHA, CW, VO and MRA, High throughput screening and analysis of screening data; HL and AA, Design, acquisition and analysis of caspase 3/7 data; BH, Design of pharmacokinetic studies and interpretation of data; PW, Conception and design, analysis and interpretation of the data, writing the manuscript.

Materials and Methods

Cell Culture

HEK293T, TREx293, U2OS, Hela, and mouse embryonic fibroblasts (MEFs) were maintained at 37^{o} C, 5% CO_2 in DMEM media supplemented with 10% FBS, L-glutamine and antibiotics (penicillin and streptomycin).

Chemicals

Tunicamycin was obtained from Calbiochem EMB Bioscience. Thapsigargin was obtained from Sigma-Aldrich. Torin-1 was obtained from Tocris Cookson Inc. The HRI activator was purchased from Maybridge (KM09748).

Generation of ATF4 reporter constructs and cell lines for small-molecule screening

ATF4 reporters were constructed by fusing the human full-length ATF4 5'-UTR (NCBI Accession BC022088.2) in front of the firefly luciferase (FLuc) or a destabilized eGFP (dEGFP) coding sequences lacking the initiator methionine.

The ATF4-FLuc reporter was generated by cloning a PCR-product containing the ATF4 full-length 5'-UTR (from +1 position a the transcription start site down to one nucleotide after the terminator codon of the second uORF) flanked by KpnI/XhoI and BglII sites at the 5' and 3' ends, respectively, into the KpnI-BglII sites of pCAX-F-XBP1-Luc (kind gift of Takao Iwawaki, RIKEN). The resulting construct, pCAX-ATF4-FLuc, was then digested with BamHI, blunted with T4 DNA polymerase, and then digested with XhoI. The resulting fragment was then subcloned into the retroviral expression vector pLPCX (Clontech) after digesting it with HindIII, blunting with T4 DNA polymerase and then digesting with XhoI to generate pLPCX-ATF4-FLuc (DAA-312). DAA-312 was used to produce recombinant retroviruses using standard methods and the resulting viral supernatant was used to transduce HEK293T cells, which were then subsequently selected with puromycin to generate a stable cell line employed in the primary screen.

The ATF4-dEGFP reporter was generated using a PCR fusion-based approach. A PCR product containing the ATF4 full-length 5' leader sequence (from +1 position a the transcription start site) fused to the eGFP coding sequence 1 nucleotide downstream of the terminator codon of the second uORF, and flanked by BamHI and EcoRI, was cloned into the cognate sites of pEGFP-N3 (Clontech) to generate pCMV-ATF4-eGFP. To destabilize the eGFP fusion protein and increase the dynamic range of the reporter, residues 422-461 of mouse ornithine decarboxylase (mODC1), corresponding to its PEST sequence (42), were fused to the C-terminus of the ATF-eGFP fusion protein. To such end, the corresponding mODC1 coding sequence was amplified by PCR and cloned into the BstXI and EcoRI sites of pCMV-ATF4-eGFP. The resulting construct was designated pCMV-ATF4-d2EGFP. To further destabilize the ATF4-d1EGFP fusion protein, alanine substitutions E428A, E430A, E431A (42) were introduced in the ODC1 PEST sequence to generate pCMV-ATF4-d1EGFP. The ATF4-d1EGFP coding sequence was then excised from the expression vector using BamHI and EcoRI and subcloned into the BglII-EcoRI sites of the retroviral expression vector pLPCX (Clontech) to generate

pLPCX-ATF4-d2EGFP. Lastly, a fusion PCR product containing the encephalomyocarditis virus internal ribosomal entry site (EMCV-IRES) upstream of the monomeric cherry (mCherry) coding sequence and flanked by EcoRI and NotI recognition sites was subcloned into the cognate sites of pLPCX-ATF4-d1EGFP, thereby generating pLPCX-ATF4-d1EGFP-IRES-mCherry (DAA-361). DAA-361 was used to produce recombinant retroviruses using standard methods and the resulting viral supernatant was used to transduce U2OS cells, which were then subsequently selected with puromycin to generate a stable cell line employed in the secondary screen.

Generation of the inducible eIF2α phosphomimetic mutant construct and cell line

The coding sequences of wild type mouse eIF2α, phosphomimetic (S51D) mutant was amplified by PCR from a mammalian expression vector (kind gift of David Ron). BamHI and EcoRI recognition sites were engineered into the primers. In addition a Kozak consensus sequence and a N-terminal FLAG epitope tag were engineered in the forward primer. The resulting PCR products were subcloned into the cognate sites of the tetracycline-inducible retroviral expression vector pRetroX-Tight-Pur-GOI (Clontech). 293T target cells stably expressing the reverse tetracycline transactivator (rtTA) were generated by standard retroviral transduction using VSV-G pseudotyped retroviruses encoding rtTA (pRetroX-Tet-On Advanced, Clontech) and selected with G418. These cells were subsequently transduced with a VSV-G pseudotyped retrovirus, encoding the eIF2α(S51D) (DAA-A681) mutant allele, resulting in a puromycin-selected, tetracycline inducible, stable cell line.

Generation of the inducible 6xHIS-3xFLAG-hsATF6-alpha cell line

6xHis-3xFLAG-hsATF6-alpha was generated by PCR from p3xFLAGCMV7.1-ATF6 (43) and cloned into pcDNA5/FRT/TO. pcDNA5/FRT/TO-6xHis-3xFLAG-hsATF6-alpha was co-transfected with pOG44 into Flp-In TRex cells (44) according to manufacturers instructions (Invitrogen). After selection with 100 μg/ml Hygromycin B (Gold Biotechnology) single colonies were isolated, expanded and tested for expression of tagged ATF6.

High-throughput Primary Screen

HEK293T cells carrying the ATF4 luciferase reporter were plated on poly-lysine coated 384 well plates (Greiner) at 30,000 cells per well. Cells were treated the next day with 100 nM thapsigargin and 10 μM of the library compounds (diversity library of 106,281 compounds) for 6 h. Luminescence was measured using One Glo (Promega) as specified by the manufacturer. The primary screen had a Z' = 0.5 and its hit rate was 0.6% (compounds were considered a hit if their luciferase readouts were beyond three standard deviations of the mean luminescence intensity of thapsigargin treated cells, which corresponded to 54% inhibition). Of these, only 187 compounds did not hit a luciferase-based XBP1 splicing reporter used as proxy to measure activation of the IRE1 branch of the UPR. Thus, these were considered unique to the PERK branch and were cherry-picked for further analysis.

High-content Microscopy-based Secondary Screen

U2OS cells carrying the ATF4-dGFP-IRES-Cherry reporter were plated in 96 well plates and treated with 100 nM Thapsigargin and 10 μM of the cherry-picked compounds for 8 h. Cells were stained with Hoechst 33258 and were visualized using an automated microscope (InCell Analyzer 2000, GE Healthcare). Data acquisition and image analyses were performed with the INCell Developer Toolbox Software, version 1.9 (GE Healthcare). Compounds that blocked induction of the ATF4-dGFP reporter, did not block the accumulation of mCherry downstream of the IRES, and were deemed non-toxic as determined by cell number measured by counting nuclei, were repurchased for further analyses.

Protein Analysis

Cells were lysed in SDS-PAGE loading buffer (1% SDS, 62.5 mM Tris-HCl pH 6.8, 10% glycerol). Lysates were sonicated and equal amounts were loaded on SDS-PAGE gels (BioRad). Proteins were transferred onto nitrocellulose and probed with primary antibodies diluted in Tris-buffered saline supplemented with 0.1% Tween 20 and 5% bovine serum albumin. The following antibodies were used: CREB-2 (C-20) (1:800), eIF2Bε (B-7) (1/500) (Santa Cruz Biotechnologies); PERK (D11A8) (1:1000), PERK (C33E10) (1:1000), eIF2α (9722) (1:1000), phospho-eIF2α (Ser51) (D9G8) XP (3398) (1:1000) (Cell Signaling Technology); XBP1s (C-terminus) (1:500) (BioLegend); phospho-S539 eIF2Bε (1/1000) (Abcam); M2 Flag (1:1000) (Sigma). An HRP-conjugated secondary antibody (Amersham) was employed to detect immune-reactive bands using enhanced chemiluminescence (SuperSignal, Thermo Scientific).

Immunofluorescence

U2OS cells were seeded on Slide Flasks (Thermo Scientific) 18 h prior to processing for immunofluorescence. Cells (60% confluent) were fixed with 4 % paraformaldehyde in PBS for 15 min. The cells were then rinsed 3 times with PBS and permeabilized with 0.3% Triton X-100. The fixed cells were rinsed 3 times with PBS and blocked for 1 h at room temperature in PBS supplemented with 0.1% Triton X-100 and 5% normal goat serum. The cells were then incubated overnight at 4^{o} C with an anti-CHOP mouse monoclonal antibody (Cell Signaling Technology L63F7) at a 1:1000 dilution in blocking buffer. The next morning the slides were washed 3 times (5 min each time) with PBST (PBS-0.1% Triton X-100). The slides were then incubated for 1 h at room temperature in a 1:500 dilution (in blocking buffer) of secondary anti-mouse antibody labeled with Alexa Dye 488 (Molecular Probes). The slides were then washed 3 additional times with PBST. The cells were then counterstained with rhodamine-phalloidin (1:1,000 in PBS) for 10 min at room temperature to reveal the actin cytoskeleton. Lastly, the slides were mounted using Vectashield (Vector) mounting medium and imaged using a Zeiss Axiovert 200M epifluorescence microscope.

Polysome Gradients

Mouse Embryonic Fibroblasts (MEFs) or TREx-293 cells expressing eIF2α(S51D) were seeded on 150 mm plates and allowed to grow to 80% confluence. Cells were then induced with 25 nM doxycycline for 14 h and subsequently treated with

the appropriate compounds for the indicated times. 100 µg/ml of cycloheximide was added to the cells for 1 min before lysis. Cells were washed twice with PBS supplemented with 100 µg/ml cycloheximide and subsequently lysed in 20 mM Tris pH 7.4, 200 mM NaCl, 15 mM MgCl, 1 mM DTT, 8% Glycerol, 100 µg/ml cycloheximide, 1% Triton X-100 and EDTA-free protease inhibitor tablets (Roche). Cells were scraped, collected, triturated with a $25^{7/8}$ gauge needle, and the homogenate was centrifuged for 10 min at 10,000 x *g*. The supernatant was loaded on a 10-50 % sucrose gradient and sedimented in a SW40 rotor at 150,000 x g for 2.4 h. The gradients were fractionated using a piston gradient fractionator (BioComp) and UV absorbance at 254 nm was monitored using a UV-Monitor (BioRad).

Alpha Screen for phospho-S51 eIF2α

U2OS cells were plated on 96 well plates and left to recover overnight. Cells were treated with either with 2 µg/ml tunicamycin or 100 nM thapsigargin in the presence or absence of 100 nM ISRIB or with ISRIB alone for the indicated and the level of eIF2α phosphorylation was determined using the AlphaScreen SureFire eIF2α(p-Ser51) Assay kit (Perkin Elmer) following the manufacturer's recommendations. Plates were read in an Envision Xcite Multilabel Reader using the standard Alpha Screen settings.

Metabolic labeling

HEK293T cells were seeded on 12 well plates, allowed to recover overnight and treated for the indicated times with the indicated compounds. The cells were subsequently switched to media lacking methionine and cysteine supplemented with the indicated compounds and 50 µCi of ^{35}S-methionine (Perkin Elmer) for 20 min. Cells were lysed by addition of SDS-PAGE loading buffer. Lysates were sonicated and equal amounts were loaded on SDS-PAGE gels (BioRad). The gel was dried and radioactive methionine incorporation was detected by exposure to a phosphor-screen and visualized with a Typhoon 9400 Variable Mode Imager (GE Healthcare).

Live Cell Imaging

T-REx293 cells carrying GFP-IRE1 were imaged as described in Li et al, PNAS (45).

Caspase3/7 Activation

Hela cells were plated in 96 well Corning plates at 0.4 x 10^4 cells / well 24 hours prior to imaging. On the day of experiment, DMEM media was replaced with F12 media with appropriate concentration of inhibitors and ER stress inducers and caspase 3/7 reagent at 1:1000 dilution (Essen Bioscience #4440). Cells were imaged in the IncuCyte FLR live cell imaging system at 2 hour intervals for 70 hours. In order to quantify the total number of cells, Vybrant DyeCycle Green staining solution (1µM) was added directly to the well immediately after the final Caspase-3/7 scan and incubated for 1 h prior to acquiring final images. Data was analyzed using IncuCyte analysis software.

qRT-PCR

U2OS cells were plated on 96 well plates and allowed to recover overnight. Cells were treated for the indicated times with the indicated compounds, lysed and cDNA was

synthesized using the PowerSYBR Green Cells-to-CT kit (Ambion) following the manufacturer's recommendations. The reactions were ran in an Opticon 2 thermal cycler (BioRad) and analyzed with the Opticon Monitor v3 software (BioRad). The following oligonucleotides were used for the amplification reaction: Human GADD34: 5'-GTAGCCTGATGGGGTGCTT -3'and 5'- TGAGGCAGCCGGAGATAC -3'; Human CHOP: 5'- AGCCAAAATCAGAGCTGGAA -3' and 5'-TGGATCAGTCTGGAAAAGCA -3'; Human GAPDH: 5'-TGGAAGATGGTGATGGGATT -3' and 5'- AGCCACATCGCTCAGACAC -3'.

TaqMan assay to measure XBP1 mRNA splicing

cDNA obtained with the PowerSYBR Green Cells-to-CT™ kit (Ambion) as described above was used for the Taqman Assay. TaqMan assays were set up using iQ Supermix (BioRad), 250 nM of each outer primer, 200 nM FAM-XBP1U probe, or 100 nM HEX-XBP1S probe. The reactions were then run on a real-time DNA Engine Opticon 2 PCR thermal cycler (BioRad) and analyzed with the Opticon Monitor v3 software (BioRad). The outer primers employed for the human XBP1unspliced/spliced (u/s) TaqMan assay were: 5'-GAAGCCAAGGGGAATGAAGT-3', and 5'-GAGATGTTCTGGAGGGGTGA-3'. TaqMan probes specific for human XBP1s or XBP1u were: 5'-FAM-CAGCACTCAGACTACGTGCACCTCTG-BHQ1-3', and 5'-HEX-TCTGCTGAGTCCGCAGCAGGTGCA-BHQ1-3'.

RNA isolation and semi-quantitative RT-PCR

Total RNA from treated or untreated HEK293T cells was extracted using TRIzol (Invitrogen) following the manufacturer's recommendations. 500 ng of total RNA were reverse transcribed using the SuperScriptVilo cDNA Synthesis kit (Invitrogen). The cDNA was diluted 1 in 10 in TE (pH = 8) and 1% of the total reaction was used as a template for the PCR amplification reactions. The XBP1 primers flank the 26-nucleotide intron and produce both spliced (222 bp) and unspliced (248 bp) amplicons. The PCR products were resolved in 2.5% agarose. The following oligonucleotides were used for the amplification reaction: for human XBP1, 5'-ACTGGGTCCAAGTTGTCCAG -3' and 5'- GGAGTTAAGACAGCGCTTGG -3'; for human GAPDH 5'-TGGAAGATGGTGATGGGATT -3' and 5'-AGCCACATCGCTCAGACAC -3'.

Pharmacokinetics of ISRIB

Intra-peritoneal (ip) route of administration was performed on 6-7 wk old female CD-1 mice (Harlan Laboratories). Animals received a single, 5mg/kg dose in groups of three mice/compound/route of administration. ISRIB was dissolved in DMSO then diluted 1:1 in Super-Refined PEG 400 (Croda). Blood (80 ul) was collected from the saphenous vein at intervals post-dosing (20 min, 1 h, 3 h, 8 h, 24 h) in EDTA containing collection tubes (Sarstadt CB300) and plasma was prepared for analysis. Compounds were detected by time-of-flight mass spectroscopy.

Intra-peritoneal (ip) route of administration was performed at a single dose of 2.5mg/kg in groups of three for each time-point (2, 6, 24 and 36h). Brain tissue samples were individually homogenized with a Tissue Tearor (Model 985-370 type2, BioSpec Products Inc, Bartlesville, OK). Approximately 300 mg of tissue was placed in 5 ml polypropylene tube, and 4 volumes of water were then added to mix. The speed scale of

Tissue Tearor was set at 3 for two minutes. After homogenization, the supernatant was analyzed by LC-MS/MS to determine their brain concentration. Plasma samples were collected prior to extraction of brain samples.

Memory studies

Eight to ten-week-old male C57BL/6J mice were used for behavioral experiments. Food and water were provided *ad libitum*, and mice were kept on a 12:12 h light/dark cycle (lights on at 08:00 h). All procedures complied with Canadian Council on Animal Care guidelines

Morris Water Maze

Mice were trained in a water pool of 100 cm diameter with a hidden platform of 10 cm diameter. Mice were handled daily for 3 days before the experiment, and the training protocol consisted of 1 swimming trial per day. Each mouse swam until it found the hidden platform or 120 s, when it was gently guided to the platform and stayed there for 10 s before being returned to the cage. Immediately after the swimming trial the mice were injected intraperitoneally with ISRIB (0.25 mg/kg in saline, 1% DMSO). For the probe test, the platform was removed and each mouse was allowed to swim for 60 s, while its swimming trajectory was monitored with a video tracking system (HVS Image, Buckingham).

Contextual fear conditioning

Mice were trained with a protocol that consisted of a 2-min period of context exploration, followed by a single foot shock of 0.35 mA for 1 s. Mice received a single injection of ISRIB (2.5 mg/kg in 50% DMSO, 50% PEG 400, IP) immediately after training and were returned to their home cage. One and 24 h after training, the mice were tested for contextual fear memory by placing the animals in the conditioning context for a 4-min period. The incidence of freezing was scored in 5-s intervals as either "freezing" or "not freezing". Percent of freezing indicates the number of intervals in which freezing was observed divided by total number of 5-s intervals. Statistical analyses were done by Student's *t* tests and one-way ANOVA followed by between-group comparisons using Tukey's posthoc test.

Cannulation and auditory fear conditioning

Male Sprague Dawley rats (275 – 350 g) were used for cannulation as described in Migues et al, 2010 (46). ISRIB (0.05 mg/ml, 0.5 μl) was infused bilaterally into the amygdala immediately after auditory fear conditioning training. The infusion was performed with a microinjector (28 gauge) connected to a Hamilton syringe with plastic tubing at a rate of 0.25 μl / min. To allow for the solution containing ISRIB to diffuse from the tip of the cannula into the tissue, the microinjector stayed in the cannula for one additional minute. Training protocol for auditory fear conditioning consisted of a 2-min period of context A exploration, followed by one pairing of a tone (5000 Hz, 75 dB, 30 s) with a co-terminating foot shock (0.75 mA, 1 s). Rats were returned to their home cage 1 min after the shock. Test for auditory fear memory consisted of a 2 min acclimatizing period to the context B (pre-CS), followed by tone presentation (CS) (2800 Hz, 85 dB, 30 s). Freezing time was measured and percent of freezing was calculated. At the end of the

experiment, cannula placement was checked by examining 50 µm brain sections stained with formal-thionin under a light microscope.

Synthesis of ISRIB

General Methods

Commercially-available reagents and solvents were used as received. Silica gel chromatography was performed using a Biotage Isolera Four flash purification system with Silicycle Silia*Sep*™ cartridges. ^{1}H NMR spectra were recorded on a Varian INOVA-400 400 MHz spectrometer. Chemical shifts are reported in δ units (ppm) relative to residual solvent peak. Coupling constants (*J*) are reported in hertz (Hz). LC-MS analyses were carried out using a Waters 2795 separations module equipped with a Waters 2996 photodiode array detector, a Waters 2424 ELS detector, a Waters micromass ZQ single quadropole mass detector, and an XBridge C18 column (5 µm, 4.6 x 50 mm).

Synthesis of Bisglycolamides

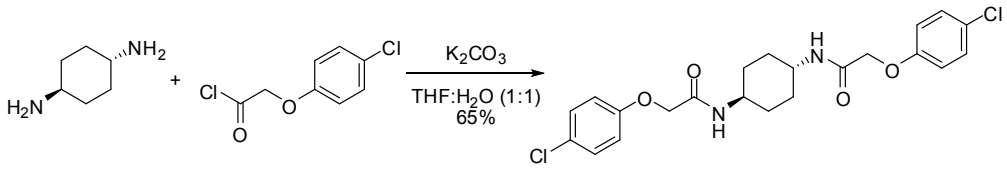

trans-ISRIB: 2-(4-Chlorophenoxy)-N-[(1r,4r)-4-[2-(4-chlorophenoxy)acetamido] cyclohexyl] acetamide

To a mixture of (1r,4r)-cyclohexane-1,4-diamine (20 mg, 0.18 mmol) in tetrahydrofuran:water (1:1, 1 ml) were sequentially added potassium carbonate (73 mg, 0.53 mmol) and 4-chlorophenoxyacetyl chloride (56 µl, 0.36 mmol). Upon addition of the acid chloride, a white solid immediately formed. The reaction mixture was vigorously stirred at ambient temperature for 30 min. Water (2.5 ml) was added. The mixture was vigorously vortexed then centrifuged, and the water was decanted. This washing protocol was repeated with potassium bisulfate (1% aq, 2.5 ml), water (2.5 ml), and diethyl ether (2 x 2.5 ml). The resulting wet white solid was dried by partially dissolving in dichloromethane/methanol (10/1, 10 ml) and gravity filtering through an Autochem 4.5 mL reaction tube. The residual undissolved product was extracted from the wet filter cake by adding dichloromethane (4 x 4.5 ml) and gravity filtering. The combined filtrate was concentrated using rotary evaporation to afford 51 mg (65%) of the title compound as a white solid. ^{1}H NMR (400 MHz, DMSO-d_6) δ 7.91 (d, J = 8.1 Hz, 2H), 7.31 (d, J = 9.0 Hz, 4H), 6.94 (d, J = 9.0 Hz, 4H), 4.42 (s, 4H), 3.55 (br. s., 2H), 1.73 (br. d, J = 5.9 Hz, 4H), 1.30 (quin, J = 10.5 Hz, 4H); LC-MS: *m/z* = 451 [M+H, ^{35}Cl x 2]$^+$, 453 [M+H, ^{35}Cl, ^{37}Cl]$^+$.

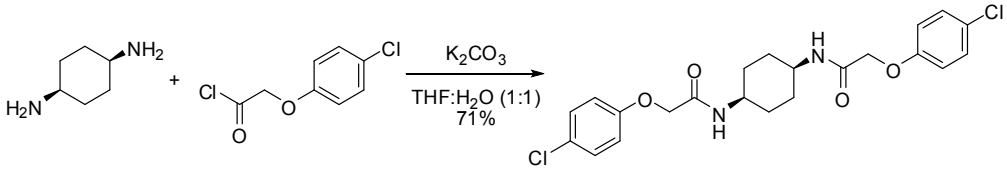

cis-ISRIB: 2-(4-chlorophenoxy)-N-[(1s,4s)-4-[2-(4-chlorophenoxy) acetamido] cyclohexyl]acetamide

To a mixture of (1s,4s)-cyclohexane-1,4-diamine (21 µl, 20 mg, 0.18 mmol) in tetrahydrofuran:water (1:1, 1 ml) were sequentially added potassium carbonate (73 mg, 0.53 mmol) and 4-chlorophenoxyacetyl chloride (56 µL, 0.36 mmol). The reaction mixture was vigorously stirred at ambient temperature for 1.5 h then partitioned between 30 mL of 1:1 dichloromethane:$KHSO_4$ (10 % aq.). After separating the organic layer, it was sequentially washed with water (1 x 10 ml) and brine (1 x 10 ml) then dried by gravity filtration using an Autochem 4.5 mL reaction tube. The filtrate was concentrated and loaded onto a Silicycle 4g SiO_2 column using a minimal amount of dichloromethane (~2 ml). The product was eluted with acetone in dichloromethane (0% - 50%). Product-containing fractions were combined and concentrated to afford 56 mg (71%) of the title compound as a white solid. ^{1}H NMR (400 MHz, DMSO-d_6) δ 7.76 (d, J = 7.0 Hz, 2H), 7.32 (d, J = 9.0 Hz, 4H), 6.94 (d, J = 9.0 Hz, 4H), 4.47 (s, 4H), 3.70 (br. s., 2H), 1.44 - 1.67 (m, 8H); LC-MS: *m/z* = 451 [M+H, ^{35}Cl x 2]$^+$, 453 [M+H, ^{35}Cl, ^{37}Cl]$^+$.

Figure Legends

Figure 1. High-throughput cell-based screen for inhibitors of PERK signaling

a. Schematic representation of the ATF4 luciferase reporter used in the primary screen. The 5' UTR of human ATF4 containing the uORFs 1 and 2 was fused to firefly luciferase and inserted into a retroviral expression system.
b. Primary screen optimization. HEK293T stably expressing the ATF4 luciferase reporter were plated in 384 well plates and treated for 6 h with 100 nM thapsigargin (Tg) or DMSO as a no ER stress control. Luciferase production was measured at the end point after 6 h (mean +/- SD). The Z' was calculated as 1- (3 (σ Tg + σ DMSO)/ (μ Tg – μ DMSO)).
c. Primary screen results. The ATF4 luciferase reporter cell line was treated for 6 h with 100 nM thapsigargin and library compounds (10 μM). Inhibition of the luciferase activity reporter was calculated as the percent reduction in relative luminescence normalized to thapsigargin treatment (0 % inhibition) and the no-ER stress control (100 % inhibition). Compounds were considered hits if they lied beyond 3 standard deviations (SD) from the thapsigargin treatment mean (red line).

Figure 2. Identification of ISRIB as a potent cell-based inhibitor of PERK signaling

a. Structures of ISRIB isosteromers.
b. Inhibition of the ATF4 luciferase reporter in HEK293T cells by ISRIB stereoisomers. Inhibition is plotted in relation to the concentration of either the *cis* or *trans* isomer of ISRIB. Cells were treated with 2 μg/ml of tunicamycin to induce ER stress and different concentrations of the inhibitors for 7 h (N = 2, mean +/- SD).
c. Effect of ISRIB on production of endogenous ATF4, PERK phosphorylation, and XBP1s production. An immunoblot analysis of PERK, ATF4 and XBP1s in HEK293T cells treated with different ER stress inducers (2.5 μg/ml tunicamycin (Tm) or 100 nM thapsigargin (Tg)) with or without 200 nM ISRIB for 3 h is shown. The arrowhead marks the XBP1s specific band.
d. Effect of ISRIB on XBP1 mRNA splicing. Taqman assays for XBP1unspliced (XBP1u) and XBP1spliced (XBP1s) on cDNA synthesized from total RNA extracted from U2OS cells treated with 2 μg/ml of tunicamycin in the presence or absence of 200 nM ISRIB for the indicated times are shown. Percent splicing was calculated as the ratio of XBP1s over total XBP1 mRNA (XBP1u + XBP1s) (mean +/- SD).

Figure 3. ISRIB makes cells resistant to eIF2α phosphorylation

a. ISRIB does not block eIF2α phosphorylation upon ER stress. eIF2α phosphorylation was measured using an Alpha-Screen Surefire eIF2α p-S51 assay (see Methods). U2OS cells were plated in 96 well plates and treated with 2 μg/ml

tunicamycin or 100 nM thapsigargin in the presence or absence of 100 nM ISRIB for the indicated times or with ISRIB alone for 120 m (N = 4, mean +/- SD). See Figure 3 supplement 1 for supporting Western blot analysis of eIF2α phosphorylation.

b. ISRIB blocks global translational attenuation observed after eIF2α phosphorylation during ER stress. HEK293T cells were treated with 100 nM thapsigargin and 200 nM ISRIB for either 1 or 3 h prior to a 20 min pulse with ^{35}S methionine before lysis. Equal amounts of lysate were loaded on an SDS-PAGE gel and quantification of radiolabeled methionine incorporation of lysates was done by gel densitometry (N = 2, SD) using Image J. (see Figure 3 supplement 2 for SDS-PAGE).
c. Polysome gradient analysis showing the block in global translational attenuation upon addition of ISRIB on ER-stressed cells. MEFs were grown in the presence or absence of 2 μg/ml of tunicamycin with or without 200 nM ISRIB for 1 h. Cell lysates were loaded on a 10-50% sucrose gradient, centrifuged at 150,000 x g for 2.4 h and absorbance at 254 nm was measured across the gradient (see Figure 3 supplement 3 for quantitation of polysome profile). A representative experiment is shown (N = 3). See Figure 3 supplement 4 for a close-up of the disome and trisome peaks.
d. Cells treated with ISRIB are resistant to the global translational attenuation exerted by forced expression of eIF2α(S51D). HEK293Trex cells were transduced with a tetracycline inducible phospho-mimetic (S51D) allele of eIF2α. Transgene expression was induced by addition of 25 nM doxycycline for 14 h in the presence or absence of 200 nM ISRIB. Lysates were collected and analyzed as described in panel c (see Figure 3 supplement 6 for quantitation of polysome profile). A representative experiment is shown (N = 2).
e. ISRIB does not reverse global translational attenuation exerted through inhibition of CAP-dependent initiation. Wild-type MEFs were treated with 750 nM Torin-1 in the presence or absence of 200 nM ISRIB for 2 h. Lysates were collected and analyzed as described in panel c. A representative experiment is shown (N = 2).
f. ISRIB blocks production of ATF4 upon GCN2 or HRI activation. An immunoblot analysis of PERK, ATF4 and total eIF2α in HEK293T cells starved for cysteine and methionine or treated with an HRI activator (6 μM) for 5 h in the presence or absence of 200 nM ISRIB is shown. Tunicamycin was used as a positive control for induction of ATF4 and the shift in PERK mobility. Under amino acid starvation we consistently observe a partial reduction of ATF4 production by ISRIB by Western blot analysis but observe a complete block in induction of the ATF4 luciferase reporter (see Figure 3 supplement 7).

Figure 4. ISRIB impairs induction of the transcriptional network controlled by ATF4

a. ER-stress dependent induction of CHOP and GADD34 mRNA is impaired in cells treated with ISRIB. qPCR analysis of total RNA extracted from U2OS cells treated with 2 μg/ml of tunicamycin in the presence or absence of 200 nM ISRIB for the indicated times. mRNA levels for each sample were normalized to

GAPDH (N = 4, mean +/- SD). p values are derived from a one-tail Student's t-test for unpaired samples. Statistical significance: CHOP, p = 0.0006 (*); GADD34, p = 0.0008 (*).

b. ISRIB blocks CHOP production during ER stress. An immunofluorescence analysis of U2OS cells treated with 100 nM thapsigargin for 2 or 4h in the presence or absence of 200 nM ISRIB is shown. A secondary Alexa Dye 488 anti-mouse antibody and rhodamine-phalloidin were used to visualize CHOP and actin, respectively.

Figure 5. ISRIB impairs adaptation to ER-stress prolonging activation of the UPR sensors

a. ISRIB sensitizes cells to acute ER stress. HEK293T cells were subjected with an acute dose of tunicamycin (2 μg/mL), ISRIB (200 nM) or a combination of both for 24 h. The treated cells were equally diluted to a concentration that would allow single cell clonal expansion and re-seeded onto 6-well plates in a 3-fold dilution series. Clonal colonies were visualized by Crystal Violet stain.
b. ISRIB synergizes with ER stress to activate caspase 3/7. Hela cells were plated in 96 well plates and treated with 5 μg/ml of tunicamycin or 500 nM thapsigargin with or without 25 nM ISRIB for the indicated times. Caspase3/7 activation was measured using Cellplayer^{TM} kinetic caspase 3/7 reagent and cells were imaged in an IncuCyte system. Green object count/mm^2 representing caspace-3/7 activation was measured at 2 h intervals (See Figure 5 Supplement 1 for endpoint quantitation of % cells with activated caspase 3/7).
c. IRE1 oligomers are sustained on ER-stressed cells treated with ISRIB. Confocal microscopy micrographs of HEK293Trex cells carrying an inducible GFP-tagged IRE1 allele were treated with 10 nM doxycycline for 24 h to induce the transgene, followed by treatment with 5 μg/ml of tunicamycin in the presence or absence of 200 nM ISRIB for the indicated times. (See Figure 5 Supplement 2 for corresponding XBP1 mRNA splicing data).
d. ATF6 cleavage is sustained in ER-stressed cells treated with ISRIB. Immunoblot analysis of ATF6 processing in HEK293Trex cells carrying an inducible FLAG epitope-tagged ATF6. Cells were treated with 50 nM doxycycline for 18 h to induce the transgene followed by treatment with 100 nM thapsigargin in the presence or absence of 200 nM ISRIB for the indicated times. Total eIF2α is used as a loading control.

Figure 6. ISRIB enhances spatial and fear-associated learning in rodents

a. Plasma concentration (ng/ml) of ISRIB after a single intraperitoneal injection (5 mg/kg). Plasma was collected at the indicated times and the concentration was determined by mass spectrometry (mean +/- SEM, N = 3).
b. Brain (ng/g tissue) and plasma concentrations (ng/ml) of ISRIB after a single intraperitoneal injection (2.5 mg/kg). Data (mean +/- SEM, N = 3) were obtained at the indicated times.

c. Escape latencies are significantly shorter in mice treated with ISRIB. Data (mean +/- SEM) were obtained in a weak 5days-long training session in the hidden platform version of the Morris water maze (1 trial per day). Mean escape latencies were plotted as a function of training days in mice treated with ISRIB (closed squares, N = 8) or vehicle (open circles N = 8) ($p < 0.05$, (*)). Mice were injected daily with ISRIB immediately after training.
d. After completion of training in the study shown in panel a, mice treated with ISRIB (black column) showed a significant preference for the target quadrant ($p < 0.05$, (*)). The probe test was performed 24 h after the last training session. p values are derived from a two-tailed Student's t test for unpaired samples.
e. After completion of training in the study shown in panel a, mice treated with ISRIB (black column) increased the number of times they crossed the platform location as compared to the vehicle-treated mice (grey column) ($p < 0.05$, (*)). P values are derived from a two-tailed Student's t test for unpaired samples.
f. Systemic administration of ISRIB (intraperitoneally after training) enhances long-term contextual fear memory (right bars, 24 h), while it does not affect short-term memory (left bars, 1 h) (N = 10 per group, $p < 0.05$, (*)). Data are presented as mean ± SEM.
g. Auditory fear conditioning is enhanced in rats treated with ISRIB. Freezing in response to a tone was assessed 3 h (short-term memory, STM, left panel) and 24 h (long-term memory, LTM, right panel) after training (vehicle-treated N = 8, and ISRIB-treated N = 7) after tone presentation (CS) and before tone presentation (pre-CS). For these experiments vehicle or ISRIB was infused directly by cannula into the amygdala after training. ISRIB-infused rats show increase freezing at 24 h ($p < 0.05$, (*)).

Supplementary Figure Legends

Figure 3 Supplement 1. ISRIB does not inhibit eIF2α phosphorylation or XBP1s production and does not lead to dephosphorylation of S539 in eIF2Bε.

Western blot analysis of PERK, ATF4, XBP1s, phospho S51-eIF2α, total eIF2α, phospho S539-eIF2Bε and total eIF2Bε in HEK293T cells treated with or without 2 μg/ml of tunicamycin or 100nM thapsigargin in the presence or absence of 200 nM ISRIB for the indicated times.

Figure 3 Supplement 2. ISRIB blocks translational attenuation upon ER stress

Autoradiogram (left) and total protein (right) obtained from HEK293T cells that were treated with 100 nM thapsigargin with or without 200 nM ISRIB for either 1 or 3 h prior to a 20 min pulse with ^{35}S methionine before lysis. Equal amounts of lysate were loaded on an SDS-PAGE gel.

Figure 3 Supplement 3. ISRIB blocks translational attenuation upon ER stress

The polysome profile in Fig 3c was quantitated by calculating the area under the curve corresponding to the monosome peak (80S), or the area under the curve corresponding to the trace covering the polysome region and then plotted as a ratio over the area under the curve corresponding to the peak of the 60S subunit.

Figure 3 Supplement 4. ISRIB partially restores the halfmer population in ER stressed cells

Wildtype MEFs were grown in the presence or absence of 2 μg/ml of tunicamycin with or without 200 nM ISRIB for 1 h. This graph is a close up of the disome and trisome peaks of the polysome gradients in Fig. 3c.

Figure 3 Supplement 5. Dissappearance of the halfmer peaks upon ER-stress is dependent on eIF2α phosphorylation

eIF2α(S51A) MEFs were grown in the presence or absence of 2 μg/ml of tunicamycin with or without 200 nM ISRIB for 1 h and polysomes gradients were processed and analyzed as described in Fig. 3c.

Figure 3 Supplement 6. ISRIB sustains translation upon expression of eIF2α(S51D)

The polysome profile in Fig. 3d was quantitated as described in Figure 3 supplement 3.

Figure 3 Supplement 7. ISRIB blocks induction of the ATF4 luciferase translational reporter upon HRI and GCN2 activation

HEK293T carrying the ATF4 luciferase reporter were treated with 2 μg/ml of tunicamycin to induce ER stress, 6 μM of the HRI activator or grown in media lacking cysteine and methionine for 7 h in the presence or absence of 200 nM ISRIB (N = 4). The relative luciferase units are normalized to the no treatment control. Using this reporter we observe a smaller fold change in production of luciferase by amino acid starvation that is fully blocked by addition of ISRIB.

Figure 5 Supplement 1. ISRIB synergizes with ER-stress to induce caspase 3/7

Green object count/mm^2 representing caspace-3/7 activation depicted in Figure 5a was normalized to the total number of cells at two different endpoints. In order to quantify the total number of cells, Vybrant DyeCycle Green staining solution (1μM) was added directly to the well immediately after the Caspase-3/7 scan and incubated for 1 h prior to acquiring final images at both 46 and 72h. Data is presented as % cells with activated caspase 3/7 at these two endpoints. Note that by 72 h the ER-stress inducing conditions used in this experiment are so detrimental that they diminish the synergistic effects observed by addition of ISRIB. The synergy was clearly seen at the 46 h time-point.

Figure 5 Supplement 2. XBP1 splicing is sustained in ER-stressed cells upon addition of ISRIB

HEK293T cells were treated with tunicamycin (2 μg/ml) for the indicated times in the presence or absence of 200 nM ISRIB. RNA was isolated from the cells and reverse transcribed followed by PCR with oligos that amplify both the unspliced and spliced versions of XBP1 mRNA or GAPDH. The DNA was electrophoresed in a 2.5% agarose gel. The asterix (*) denotes a hybrid PCR product.

References

1. Wek RC, Jiang H-Y, Anthony TG. Coping with stress: eIF2 kinases and translational control. Biochem. Soc. Trans. 2006 Feb;34(Pt 1):7–11.

2. Hinnebusch AG, Lorsch JR. The mechanism of eukaryotic translation initiation: new insights and challenges. Cold Spring Harb Perspect Biol. 2012;4(10).

3. Krishnamoorthy T, Pavitt GD, Zhang F, Dever TE, Hinnebusch AG. Tight binding of the phosphorylated alpha subunit of initiation factor 2 (eIF2alpha) to the regulatory subunits of guanine nucleotide exchange factor eIF2B is required for inhibition of translation initiation. Mol Cell Biol. 2001 Aug;21(15):5018–30.

4. Hinnebusch AG. Translational regulation of GCN4 and the general amino acid control of yeast. Annu. Rev. Microbiol. 2005;59:407–50.

5. Jackson RJ, Hellen CUT, Pestova TV. The mechanism of eukaryotic translation initiation and principles of its regulation. Nat Rev Mol Cell Biol. 2010 Feb 1;11(2):113–27.

6. Harding HP, Novoa I, Zhang Y, Zeng H, Wek R, Schapira M, et al. Regulated translation initiation controls stress-induced gene expression in mammalian cells. Mol Cell. 2000 Nov;6(5):1099–108.

7. Palam LR, Baird TD, Wek RC. Phosphorylation of eIF2 facilitates ribosomal bypass of an inhibitory upstream ORF to enhance CHOP translation. Journal of Biological Chemistry. 2011 Apr 1;286(13):10939–49.

8. Vattem KM, Wek RC. Reinitiation involving upstream ORFs regulates ATF4 mRNA translation in mammalian cells. Proc Natl Acad Sci USA. 2004 Aug 3;101(31):11269–74.

9. Ma Y, Brewer JW, Diehl JA, Hendershot LM. Two distinct stress signaling pathways converge upon the CHOP promoter during the mammalian unfolded protein response. J. Mol. Biol. 2002 May 17;318(5):1351–65.

10. Pavitt GD, Ron D. New insights into translational regulation in the endoplasmic reticulum unfolded protein response. Cold Spring Harb Perspect Biol. 2012

Jun;4(6).

11. Ron D, Walter P. Signal integration in the endoplasmic reticulum unfolded protein response. Nat Rev Mol Cell Biol. 2007 Jul;8(7):519–29.

12. Gardner BM, Walter P. Unfolded proteins are Ire1-activating ligands that directly induce the unfolded protein response. Science. 2011 Sep 30;333(6051):1891–4.

13. Harding HP, Zhang Y, Bertolotti A, Zeng H, Ron D. Perk is essential for translational regulation and cell survival during the unfolded protein response. Mol Cell. 2000 May;5(5):897–904.

14. Walter P, Ron D. The unfolded protein response: from stress pathway to homeostatic regulation. Science. 2011 Nov 25;334(6059):1081–6.

15. Tabas I, Ron D. Integrating the mechanisms of apoptosis induced by endoplasmic reticulum stress. Nat Cell Biol. 2011 Mar 1;13(3):184–90.

16. Shore GCG, Papa FRF, Oakes SAS. Signaling cell death from the endoplasmic reticulum stress response. Current Opinion in Cell Biology. 2011 Apr 1;23(2):143–9.

17. Thoreen CC, Chantranupong L, Keys HR, Wang T, Gray NS, Sabatini DM. A unifying model for mTORC1-mediated regulation of mRNA translation. Nature. 2012 May 3;485(7396):109–13.

18. Chen T, Ozel D, Qiao Y, Harbinski F, Chen L, Denoyelle S, et al. Chemical genetics identify eIF2α kinase heme-regulated inhibitor as an anticancer target. Nature Chemical Biology. 2011 Sep 1;7(9):610–6.

19. Lu PD, Jousse C, Marciniak SJ, Zhang Y, Novoa I, Scheuner D, et al. Cytoprotection by pre-emptive conditional phosphorylation of translation initiation factor 2. EMBO J. 2004 Jan 14;23(1):169–79.

20. Salvesen GS, Ashkenazi A. Snapshot: caspases. Cell. 2011 Oct 14;147(2):476–476.e1.

21. Jiang Z, Belforte JE, Lu Y, Yabe Y, Pickel J, Smith CB, et al. eIF2alpha Phosphorylation-dependent translation in CA1 pyramidal cells impairs hippocampal memory consolidation without affecting general translation. Journal of Neuroscience. 2010 Feb 17;30(7):2582–94.

22. Costa-Mattioli M, Gobert D, Stern E, Gamache K, Colina R, Cuello C, et al. eIF2alpha phosphorylation bidirectionally regulates the switch from short- to long-term synaptic plasticity and memory. Cell. 2007 Apr 6;129(1):195–206.

23. Vazquez de Aldana CR, Hinnebusch AG. Mutations in the GCD7 subunit of yeast guanine nucleotide exchange factor eIF-2B overcome the inhibitory effects of

phosphorylated eIF-2 on translation initiation. Mol Cell Biol. 1994 May;14(5):3208–22.

24. Pavitt GD, Ramaiah KV, Kimball SR, Hinnebusch AG. eIF2 independently binds two distinct eIF2B subcomplexes that catalyze and regulate guanine-nucleotide exchange. Genes Dev. 1998 Feb 15;12(4):514–26.

25. Pavitt GD, Yang W, Hinnebusch AG. Homologous segments in three subunits of the guanine nucleotide exchange factor eIF2B mediate translational regulation by phosphorylation of eIF2. Mol Cell Biol. 1997 Mar;17(3):1298–313.

26. Woo CW, Kutzler L, Kimball SR, Tabas I. Toll-like receptor activation suppresses ER stress factor CHOP and translation inhibition through activation of eIF2B. Nat Cell Biol. 2012 Feb 1;14(2):192–200.

27. Woo CW, Cui D, Arellano J, Dorweiler B, Harding H, Fitzgerald KA, et al. Adaptive suppression of the ATF4-CHOP branch of the unfolded protein response by toll-like receptor signalling. Nat Cell Biol. 2009 Dec;11(12):1473–80.

28. Harding HP, Zhang Y, Zeng H, Novoa I, Lu PD, Calfon M, et al. An integrated stress response regulates amino acid metabolism and resistance to oxidative stress. Mol Cell. 2003 Mar;11(3):619–33.

29. Axten JM, Medina JR, Feng Y, Shu A, Romeril SP, Grant SW, et al. Discovery of 7-methyl-5-(1-{[3-(trifluoromethyl)phenyl]acetyl}-2,3-dihydro-1H-indol-5-yl)-7H-pyrrolo[2,3-d]pyrimidin-4-amine (GSK2606414), a potent and selective first-in-class inhibitor of protein kinase R (PKR)-like endoplasmic reticulum kinase (PERK). J Med Chem. 2012 Aug 23;55(16):7193–207.

30. Bi M, Naczki C, Koritzinsky M, Fels D, Blais J, Hu N, et al. ER stress-regulated translation increases tolerance to extreme hypoxia and promotes tumor growth. EMBO J. 2005 Oct 5;24(19):3470–81.

31. Ye J, Kumanova M, Hart LS, Sloane K, Zhang H, De Panis DN, et al. The GCN2-ATF4 pathway is critical for tumour cell survival and proliferation in response to nutrient deprivation. EMBO J. 2010 Jun 16;29(12):2082–96.

32. Li W, Wang X, Van Der Knaap MS, Proud CG. Mutations Linked to Leukoencephalopathy with Vanishing White Matter Impair the Function of the Eukaryotic Initiation Factor 2B Complex in Diverse Ways. Mol Cell Biol. 2004 Apr 15;24(8):3295–306.

33. Borck G, Shin B-S, Stiller B, Mimouni-Bloch A, Thiele H, Kim J-R, et al. eIF2γ Mutation that Disrupts eIF2 Complex Integrity Links Intellectual Disability to Impaired Translation Initiation. Mol Cell. 2012 Oct.

34. Costa-Mattioli M, Gobert D, Harding H, Herdy B, Azzi M, Bruno M, et al. Translational control of hippocampal synaptic plasticity and memory by the

eIF2alpha kinase GCN2. Nature. 2005 Aug 25;436(7054):1166–73.

35. Zhu PJ, Huang W, Kalikulov D, Yoo JW, Placzek AN, Stoica L, et al. Suppression of PKR Promotes Network Excitability and Enhanced Cognition by Interferon-γ-Mediated Disinhibition. Cell. 2011 Dec 9;147(6):13–3.

36. Sutton MA, Schuman EM. Dendritic protein synthesis, synaptic plasticity, and memory. Cell. 2006 Oct 6;127(1):49–58.

37. Klann E, Dever TE. Biochemical mechanisms for translational regulation in synaptic plasticity. Nat. Rev. Neurosci. 2004 Dec;5(12):931–42.

38. Bartsch D, Ghirardi M, Skehel PA, Karl KA, Herder SP, Chen M, et al. Aplysia CREB2 represses long-term facilitation: relief of repression converts transient facilitation into long-term functional and structural change. Cell. 1995 Dec 15;83(6):979–92.

39. Yin JC, Wallach JS, Del Vecchio M, Wilder EL, Zhou H, Quinn WG, et al. Induction of a dominant negative CREB transgene specifically blocks long-term memory in Drosophila. Cell. 1994 Oct 7;79(1):49–58.

40. Chen A, Muzzio IA, Malleret G, Bartsch D, Verbitsky M, Pavlidis P, et al. Inducible enhancement of memory storage and synaptic plasticity in transgenic mice expressing an inhibitor of ATF4 (CREB-2) and C/EBP proteins. Neuron. 2003 Aug 14;39(4):655–69.

41. Trinh MAM, Kaphzan HH, Wek RCR, Pierre PP, Cavener DRD, Klann EE. Brain-specific disruption of the eIF2α kinase PERK decreases ATF4 expression and impairs behavioral flexibility. Cell Rep. 2012 Jun 28;1(6):676–88.

42. Li X, Zhao X, Fang Y, Jiang X, Duong T, Fan C, et al. Generation of destabilized green fluorescent protein as a transcription reporter. J Biol Chem. 1998 Dec 25;273(52):34970–5.

43. Shen J, Chen X, Hendershot L, Prywes R. ER stress regulation of ATF6 localization by dissociation of BiP/GRP78 binding and unmasking of Golgi localization signals. Developmental Cell. 2002 Jul;3(1):99–111.

44. Cohen HR, Panning B. XIST RNA exhibits nuclear retention and exhibits reduced association with the export factor TAP/NXF1. Chromosoma. 2007 Aug;116(4):373–83.

45. Li H, Korennykh AV, Behrman SL, Walter P. Mammalian endoplasmic reticulum stress sensor IRE1 signals by dynamic clustering. Proceedings of the National Academy of Sciences. 2010 Sep 14;107(37):16113–8.

46. Migues PV, Hardt O, Wu DC, Gamache K, Sacktor TC, Wang YT, et al. PKMzeta maintains memories by regulating GluR2-dependent AMPA receptor trafficking.

Nat. Neurosci. 2010 May;13(5):630–4.

Figure 1

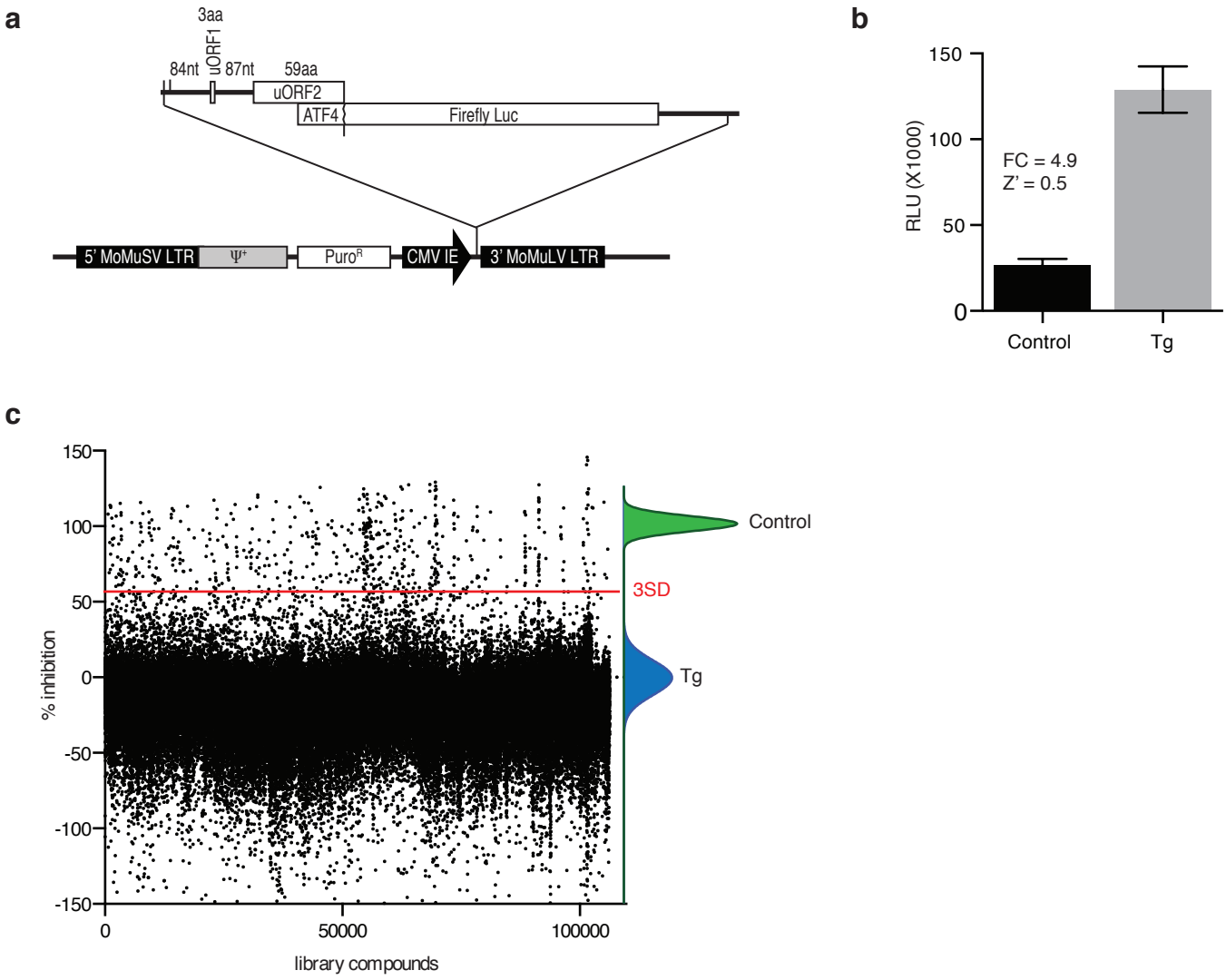
a
3aa
uORF1
84nt
87nt
59aa
uORF2
ATF4
Firefly Luc
5' MoMuSV LTR
Ψ+
Puro^R
CMV IE
3' MoMuLV LTR
b
RLU (X1000)
150
100
50
0
FC = 4.9
Z' = 0.5
Control
Tg
c
% inhibition
150
100
50
0
-50
-100
-150
0
50000
100000
library compounds
Control
3SD
Tg

Figure 2

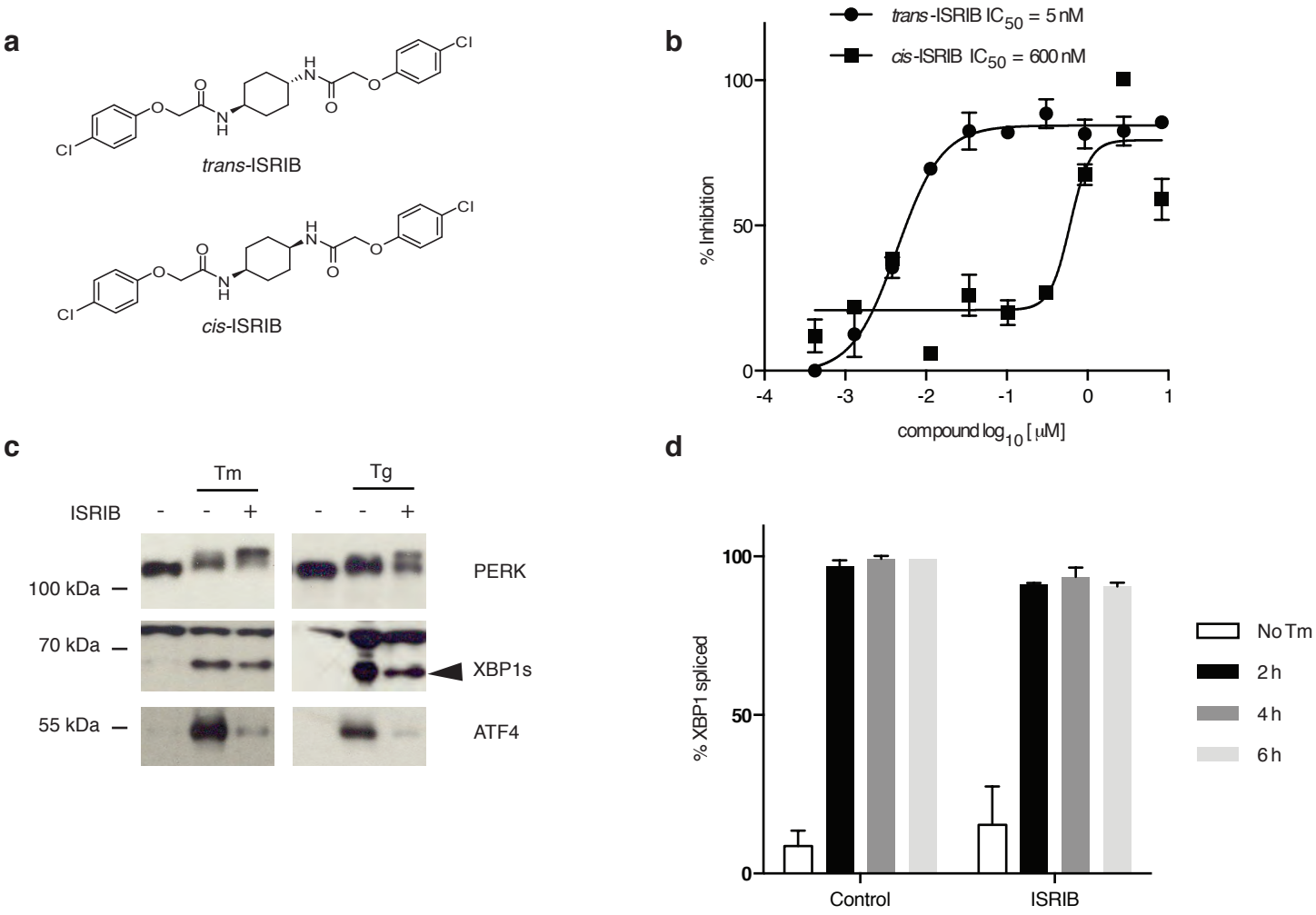
a
trans-ISRIB
cis-ISRIB
b
trans-ISRIB IC50 = 5 nM
cis-ISRIB IC50 = 600 nM
% Inhibition
compound log10 [μM]
c
Tm
Tg
ISRIB
100 kDa
70 kDa
55 kDa
PERK
XBP1s
ATF4
d
% XBP1 spliced
No Tm
2 h
4 h
6 h
Control
ISRIB

Figure 3

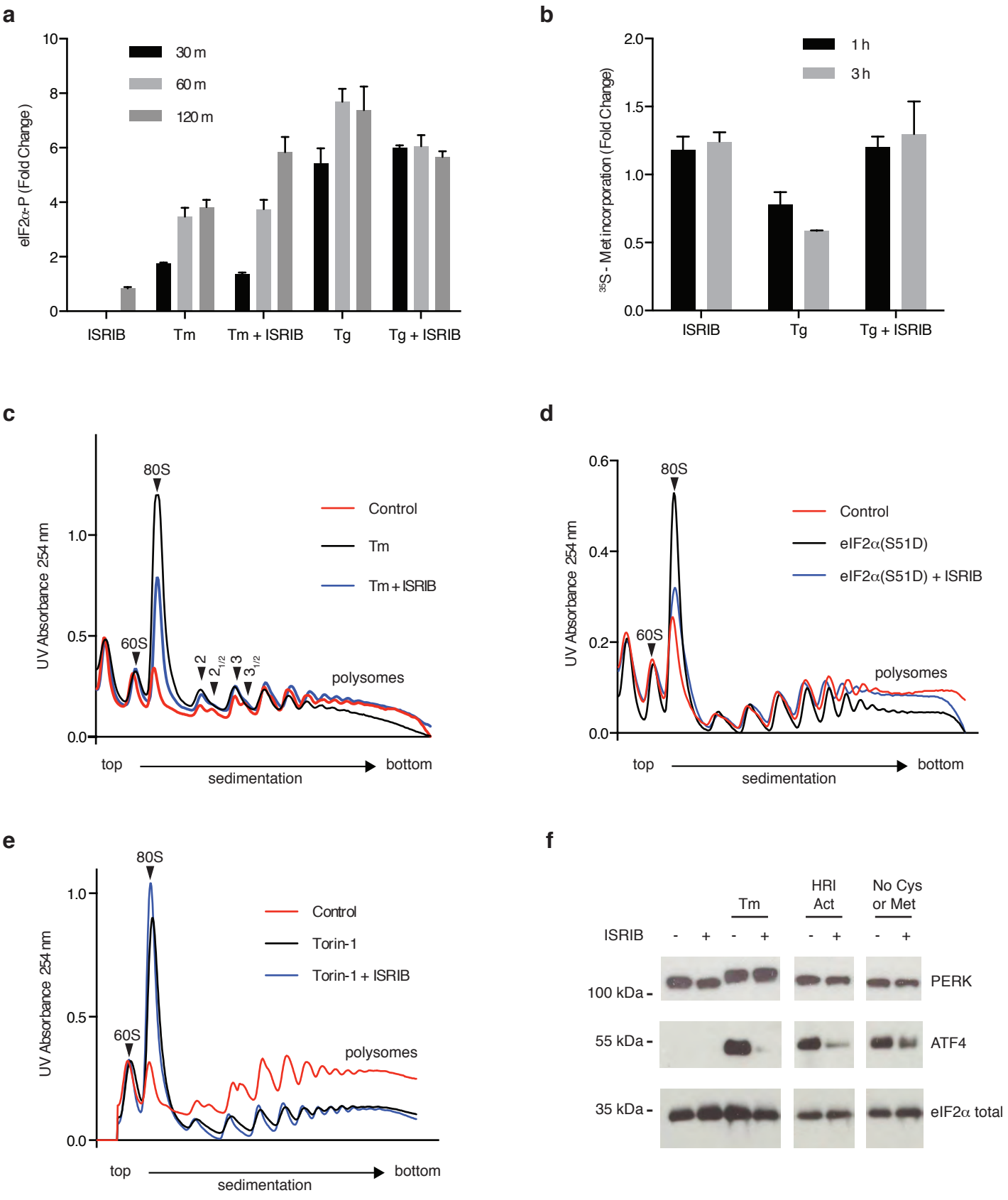
a
eIF2α-P (Fold Change)
30 m
60 m
120 m
ISRIB
Tm
Tm + ISRIB
Tg
Tg + ISRIB
b
35S - Met incorporation (Fold Change)
1 h
3 h
ISRIB
Tg
Tg + ISRIB
c
UV Absorbance 254 nm
80S
60S
2
2 1/2
3
3 1/2
Control
Tm
Tm + ISRIB
polysomes
top
sedimentation
bottom
d
UV Absorbance 254 nm
80S
60S
Control
eIF2α(S51D)
eIF2α(S51D) + ISRIB
polysomes
top
sedimentation
bottom
e
UV Absorbance 254 nm
80S
60S
Control
Torin-1
Torin-1 + ISRIB
polysomes
top
sedimentation
bottom
f
Tm
HRI Act
No Cys or Met
ISRIB
100 kDa
55 kDa
35 kDa
PERK
ATF4
eIF2α total

Figure 4

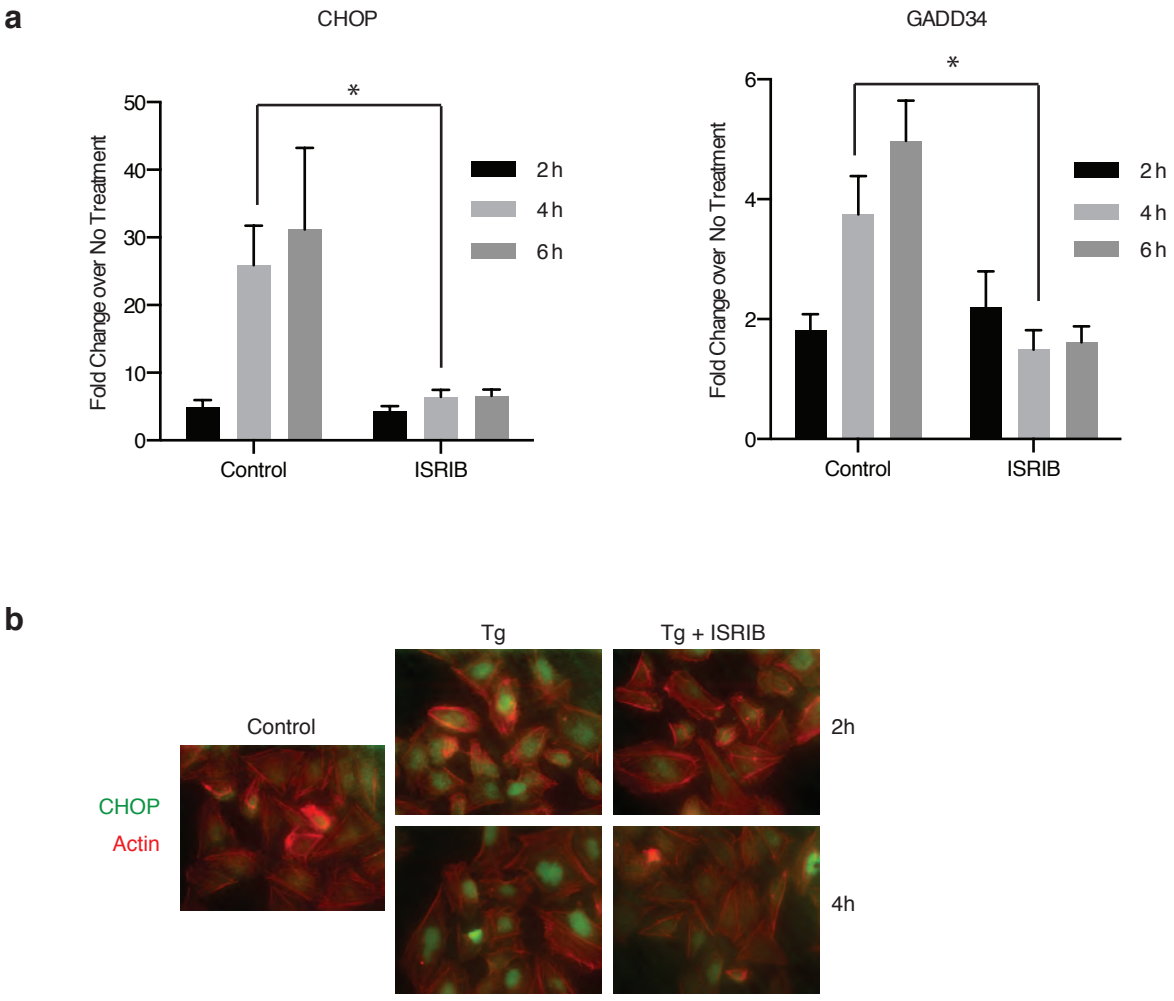
a
CHOP
GADD34
Fold Change over No Treatment
50
40
30
20
10
0
6
4
2
*
2 h
4 h
6 h
Control
ISRIB
b
Tg
Tg + ISRIB
Control
2h
4h
CHOP
Actin

Figure 5

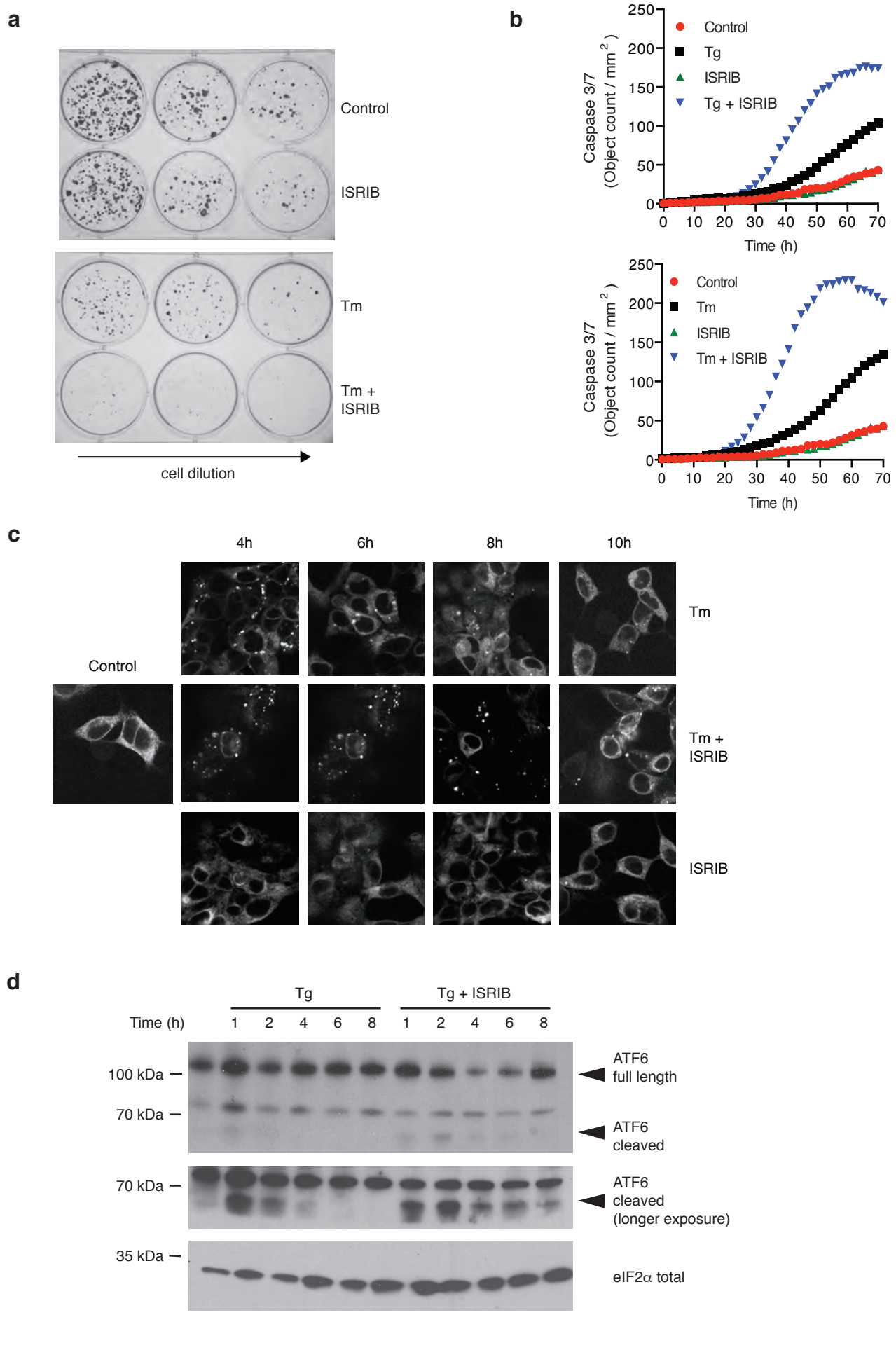
a
Control
ISRIB
Tm
Tm +
ISRIB
cell dilution
b
Caspase 3/7
(Object count / mm 2)
Control
Tg
ISRIB
Tg + ISRIB
Time (h)
Control
Tm
ISRIB
Tm + ISRIB
c
4h
6h
8h
10h
Control
Tm
Tm +
ISRIB
ISRIB
d
Tg
Tg + ISRIB
Time (h)
1 2 4 6 8 1 2 4 6 8
100 kDa
70 kDa
ATF6
full length
ATF6
cleaved
70 kDa
ATF6
cleaved
(longer exposure)
35 kDa
eIF2α total

Figure 6

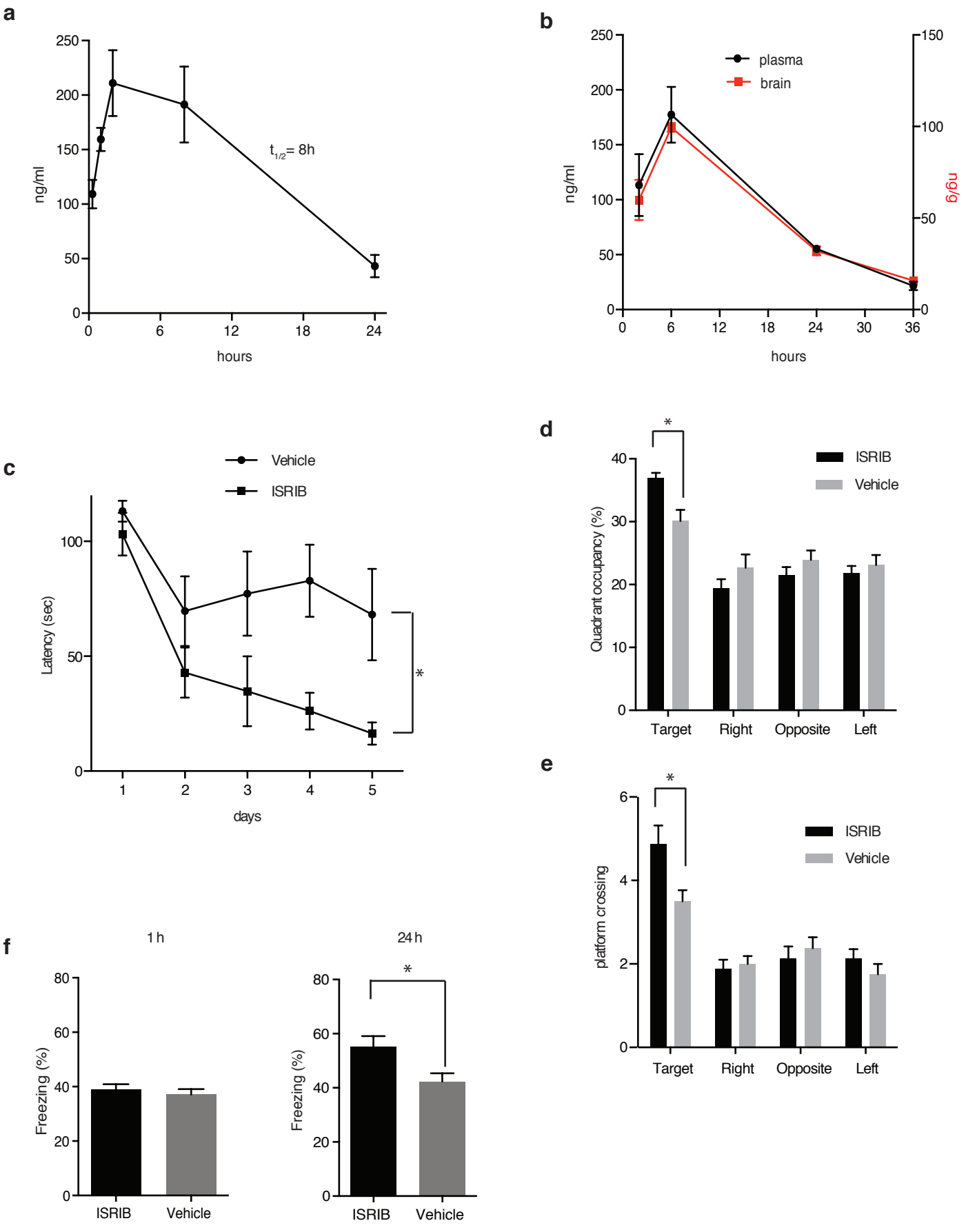
a
ng/ml
hours
$t_{1/2}$= 8h
b
plasma
brain
ng/ml
ng/g
hours
c
Vehicle
ISRIB
Latency (sec)
days
*
d
ISRIB
Vehicle
Quadrant occupancy (%)
Target
Right
Opposite
Left
*
e
ISRIB
Vehicle
platform crossing
Target
Right
Opposite
Left
*
f
1 h
24 h
Freezing (%)
ISRIB
Vehicle
*

Figure 6

g

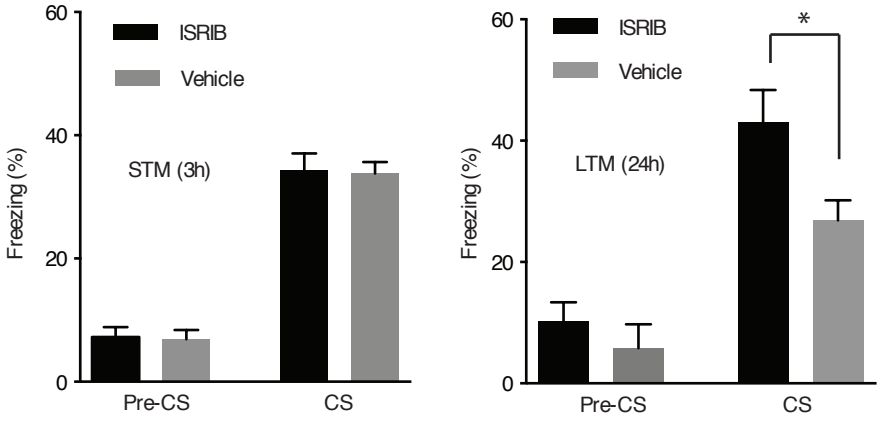
60
40
20
0
Freezing (%)
ISRIB
Vehicle
STM (3h)
Pre-CS
CS
60
40
20
0
Freezing (%)
ISRIB
Vehicle
LTM (24h)
*
Pre-CS
CS

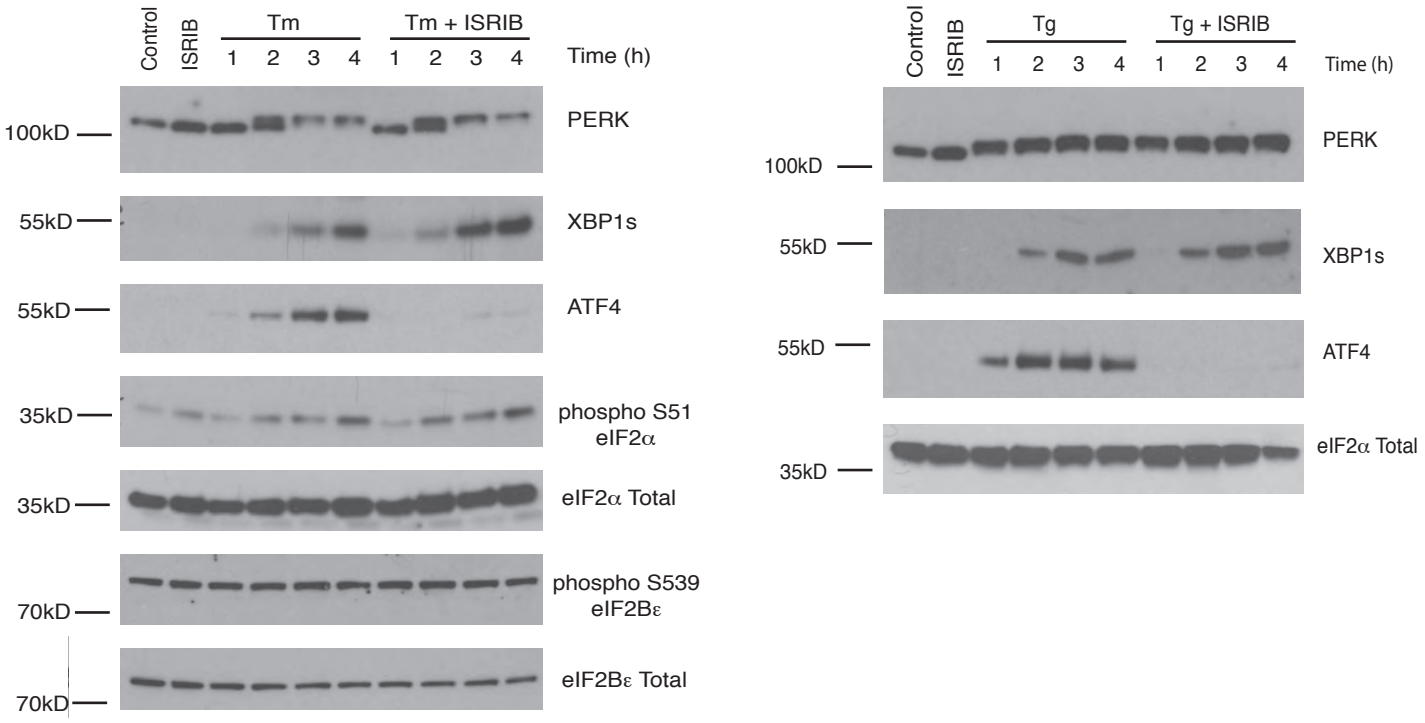

Figure 3 Supplement 1. ISRIB does not inhibit eIF2α phosphorylation or XBP1s production

Western blot analysis of PERK, ATF4, XBP1s, phospho S51-eIF2α, total eIF2α, phospho S539-eIF2Bε and total eIF2Bε in HEK293T cells treated with or without 2 μg/ml of tunicamycin or 100nM thapsigargin in the presence or absence of 200 nM ISRIB for the indicated times.

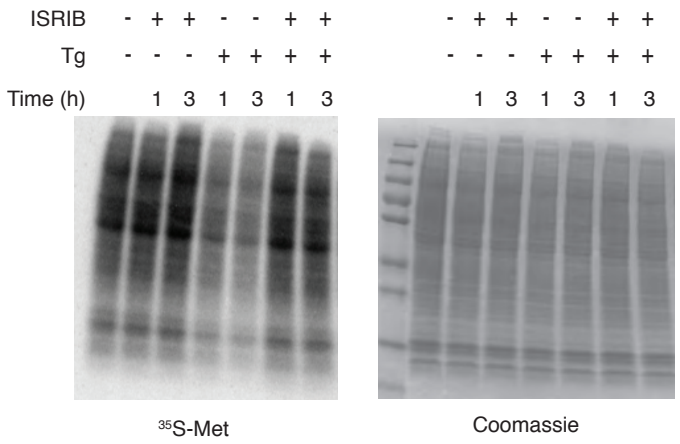

Figure 3 Supplement 2. ISRIB blocks translational attenuation upon ER stress

Autoradiogram (left) and total protein (right) obtained from HEK293T cells that were treated with 100 nM thapsigargin with or without 200 nM ISRIB for either 1 or 3 h prior to a 20 min pulse with ^{35}S methionine before lysis. Equal amounts of lysate were loaded on an SDS-PAGE gel.

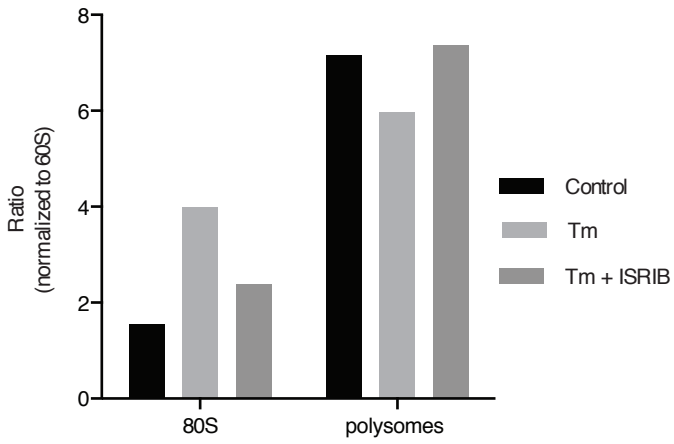

Figure 3 Supplement 3. ISRIB blocks translational attenuation upon ER stress

The polysome profile in Fig 3c was quantitated by calculating the area under the curve corresponding to the monosome peak (80S), or the area under the curve corresponding to the trace covering the polysome region and then plotted as a ratio over the area under the curve corresponding to the peak of the 60S subunit.

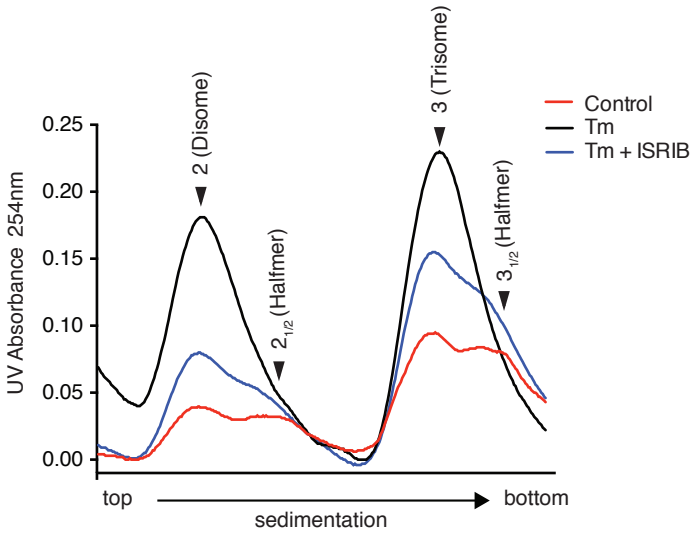

Figure 3 Supplement 4. ISRIB partially restores the halfmer population in ER stressed cells

Wildtype MEFs were grown in the presence or absence of 2 μg/ml of tunicamycin with or without 200 nM ISRIB for 1 h. This graph is a close up of the disome and trisome peaks of the polysome gradient in Fig. 3c after normalization of the curves.

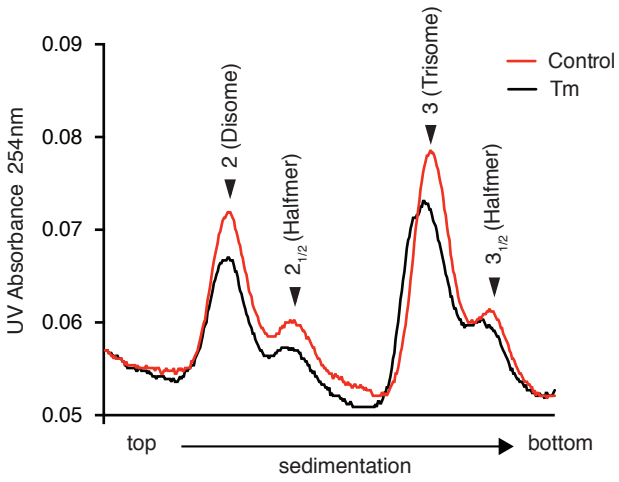

Figure 3 Supplement 5. Disappearance of the halfmer peaks upon ER-stress is dependent on eIF2α phosphorylation

eIF2α(S51A) MEFs were grown in the presence or absence of 2 μg/ml of tunicamycin with or without 200 nM ISRIB for 1 h and polysomes gradients were processed and analyzed as described in Fig. 3c.

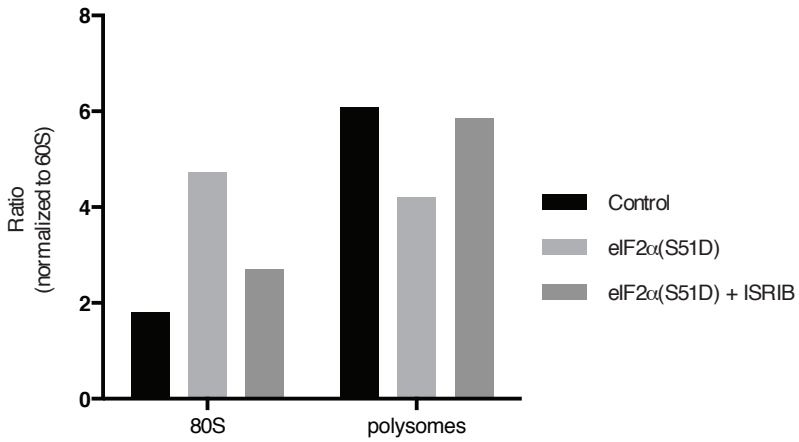

Figure 3 Supplement 6. ISRIB sustains translation upon expression of eIF2α(S51D)

The polysome profile in Fig. 3d was quantitated as described in Figure 3 supplement 3.

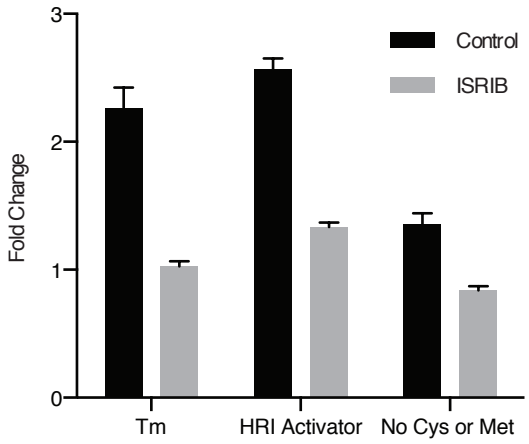

Figure 3 Supplement 7. ISRIB blocks induction of the ATF4 luciferase translational reporter upon HRI and GCN2 activation

HEK293T carrying the ATF4 luciferase reporter were treated with 2 μg/ml of tunicamycin to induce ER stress, 6 μM of the HRI activator or grown in media lacking cysteine and methionine for 7 h in the presence or absence of 200 nM ISRIB (N = 4). The relative luciferase units are normalized to the no treatment control. Using this reporter we observe a smaller fold change in production of luciferase by amino acid starvation that is fully blocked by addition of ISRIB.

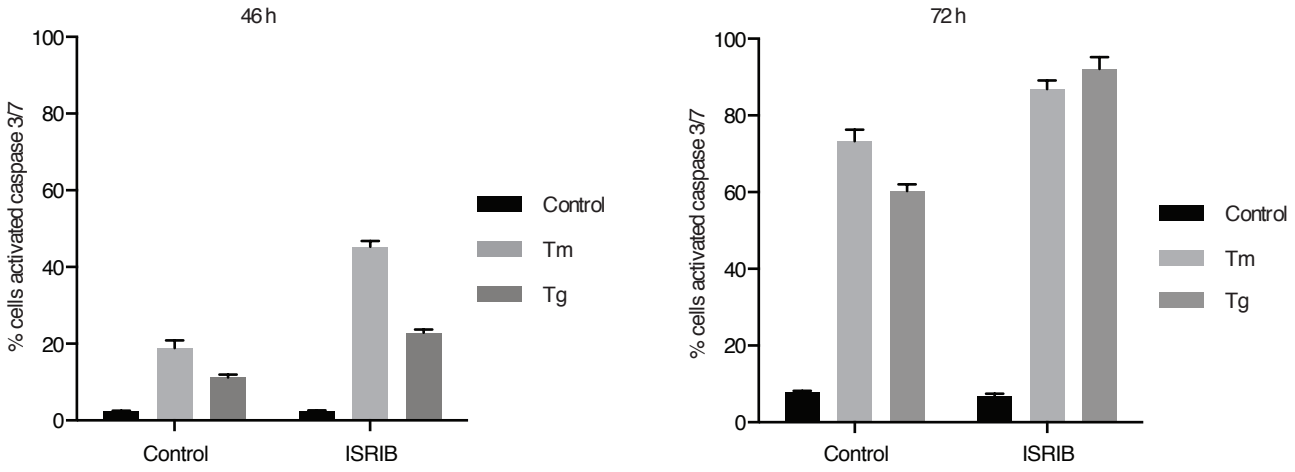

Figure 5 Supplement 1. ISRIB synergizes with ER-stress to induce caspase 3/7

Green object count/mm^2 representing caspace-3/7 activation depicted in Fig. 5a was normalized to the total number of cells at two different endpoints. In order to quantify the total number of cells, Vybrant DyeCycle Green staining solution (1μM) was added directly to the well immediately after the Caspase-3/7 scan and incubated for 1 h prior to acquiring final images at both 46 and 72h. Data is presented as % cells with activated caspase 3/7 at these two endpoints. Note that by 72 h the ER-stress inducing conditions used in this experiment are so detrimental that they diminish the synergistic effects observed by addition of ISRIB. The synergy was clearly seen at the 46 h time-point.

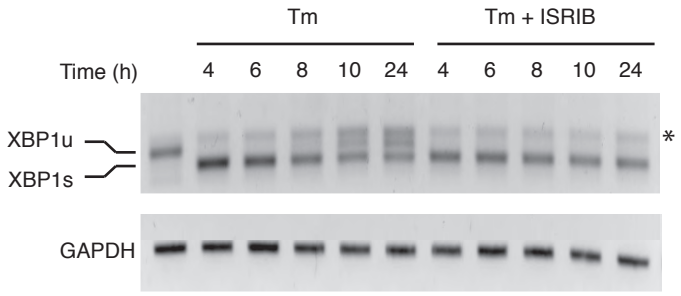

Figure 5 Supplement 2. XBP1 splicing is sustained in ER-stressed cells upon addition of ISRIB

HEK293T cells were treated with tunicamycin (2 μg/ml) for the indicated times in the presence or absence of 200 nM ISRIB. RNA was isolated from the cells and reverse transcribed followed by PCR with oligos that amplify both the unspliced and spliced versions of XBP1 mRNA or GAPDH. The DNA was electrophoresed in a 2.5% agarose gel. The asterix (*) denotes a hybrid PCR product.